Coordination Chemistry Reviews 253 (2009) 2787–2804

Contents lists available at ScienceDirect

Coordination Chemistry Reviews

journal homepage: www.elsevier.com/locate/ccr

Review

Structural overview and structure–property relationships of iodoplumbate and iodobismuthate

Contents

* Corresponding author. Tel.: +86 591 83704947; fax: +86 591 83704947.
E-mail address: chenl@fjirsm.ac.cn (L. Chen).

0010-8545/$ – see front matter © 2009 Elsevier B.V. All rights reserved.
doi:10.1016/j.ccr.2009.08.003

ARTICLE INFO

Article history:
Received 10 April 2009
Accepted 5 August 2009
Available online 12 August 2009

Keywords:
Lead
Bismuth
Iodoplumbate
Iodobismuthate
Heterometallic iodometalate
Structure–property relationship

ABSTRACT

This review discusses the main structural features of the inorganic of the iodoplumbate and iodobismuthate moieties according to the aggregation and connections of the primary MI_6 octahedron building unit. The cation effect, ligand effect and hetero metal–iodine bonding effect are summarized. The aggregation density of the inorganic moiety (ADIM) is an important structural parameter that is related to the solid-state properties. An empirical r value is thus defined as $r = \Sigma(N\mu_n\text{-I})/n$, where $N\mu_n$-I means the number of n-fold-coordinated I atoms per building unit and n = 1–6; M/r value as $M/r = M{:}r$ (M = the number of metal centers per building unit). The M/r value–anionic structure relationship and M/r value–band gap correlation are described. Several interesting optical, thermal and ferroelectric properties that are related to the dimensionality, composition, configuration, distortion, and bonding are discussed in detail.

© 2009 Elsevier B.V. All rights reserved.

1. Introduction

Binary PbI_2 and BiI_3 are interesting semiconductors. Hexagonal PbI_2 has a layered structure, in which each Pb atom has an octahedral PbI_6^{4-} coordination sphere that is condensed to layers by sharing edges with six neighboring octahedra [1]. BiI_3 crystallizes in a PbI_2-like trigonal structure, in which one-third of the metallic sites are empty so as to balance the lower Bi:I ratio [2]. Both PbI_2 and BiI_3 show interesting properties, such as electroluminescence [3], photoluminescence [4,5], and nonlinear optical effects [6], and are good candidates for room temperature X-ray or γ-ray detectors [7–9] and thin film transistors [10]. Recently, the Pb-, Bi-related iodometalates have also been intensively studied for their diversity of structures [11–14] and interesting optical and electronic properties, such as luminescence [15,16], nonlinear optical activity [17,18], semiconductivity (even metallic conductivity) [19,20], and ferroelectricity [21]. Interestingly, some of these properties originated from the binary iodides; some new ones are generated by their novel derivative structures.

Similar to that in the binary, the MI_6^{n-} (M = Pb, Bi) octahedra are the most common building units in iodometalates. Both Pb and Bi have large atomic numbers and radii, so the energy levels of the outermost s and p orbitals are greatly different. Therefore, these two atoms lose only p electrons and yield stable s^2 Pb^{2+} and Bi^{3+} ions, respectively. The nucleus of Pb^{2+} and Bi^{3+} weakly binds the outer s electrons, so the Pb^{2+} and Bi^{3+} ions are soft or polarizable, which essentially allows a great degree of distortion and aggregation of the MI_x^{n-} polyhedron. In addition, compared with M–O or M–S bonds in oxometalates and thiometalates, the covalency of M–I bonds is relatively weak. Thus, the Pb–I and Bi–I covalent bonds exhibit low directional-correlations. Therefore, the MI_x octahedron has a great tendency to form structures with distortion, vacancy and aggregation, through which various novel iodometalate structures can be built.

The structural diversity of the inorganic moieties of iodoplumbate and iodobismuthate is remarkable. Presently, the structural modifications of the inorganic moiety have been achieved by the adjustment of dimensionality, aggregation, distortion, involvement of heterometallic bonding interactions beyond the Bi–I or Pb–I bonds, and effect of ligand that are directly coordinated to the inorganic part. The structural comparison of these inorganic moieties has nicely demonstrated the growth from discrete building units to polymeric 1D, 2D or 3D species. Some of these new structures generate novel properties, so that the Pb/Bi iodometalates can be ideal systems to study structure–property relationships. A thorough understanding of the structural chemistry is the first step towards the rational syntheses of target compounds with desired properties.

2. Structural description and comparison between iodoplumbate and iodobismuthate

The major structural characteristic of iodoplumbate and iodobismuthate is the diverse anionic structure motif, which ranges from discrete mono- or polynuclear species to infinite variety with higher dimensionality (1D, 2D, or 3D). The stepwise aggregations of MI_6 octahedra are impressively shown in the 0D iodometalates. Similarly, the one-dimensional iodometalate chains can also be made from MI_6 octahedral units through sharing I–I–I faces, I–I edges or I apexes. Furthermore, connections in two or three different directions can lead to 2D polymer or 3D networks. Representative examples are discussed in the following sections.

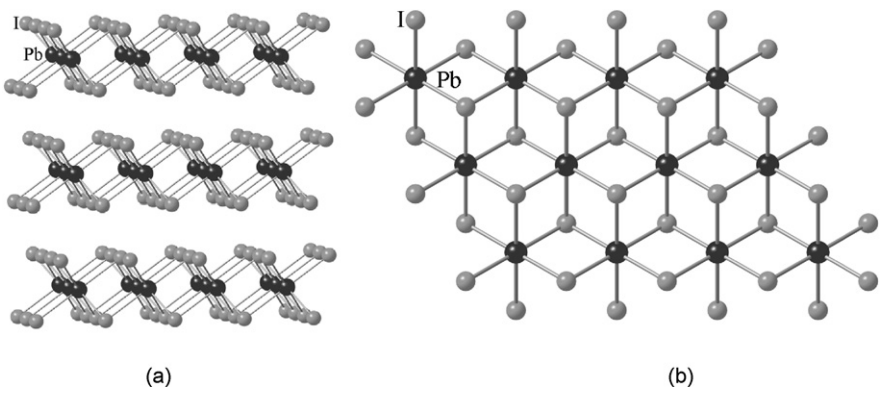

Fig. 1. Structure of PbI_2: (a) packing diagram and (b) layered structure of (0 0 1) view [1].

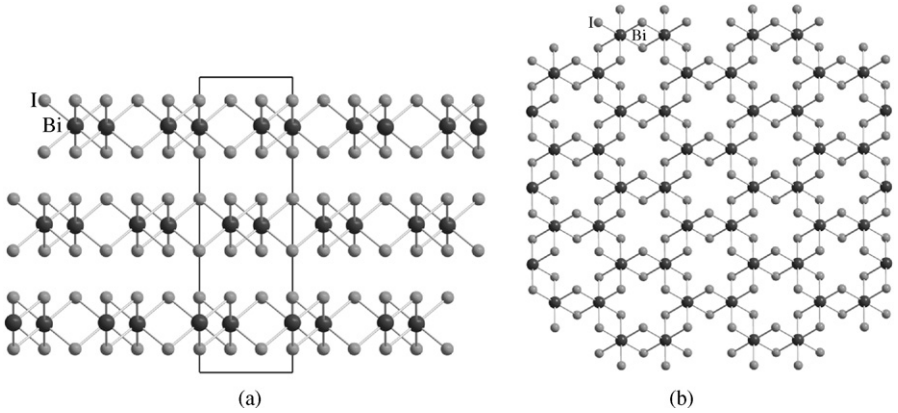

Fig. 2. Structure of BiI_3: (a) packing diagram and (b) layered structure of (0 0 1) view [2].

2.1. Binary PbI_2 and BiI_3

Hexagonal PbI_2 has a layered structure with $a = b = 4.557$ Å, and $c = 6.979$ Å (Fig. 1). Each Pb atom has an octahedral PbI_6 coordination sphere that is condensed to layers by sharing edges with six neighboring octahedra. Bulk PbI_2 is yellow powder, melts at 405 °C, and has an optical energy gap of about 2.3 eV [1]. BiI_3 crystallizes in a trigonal structure with $a = b = 7.525$ Å, and $c = 20.703$ Å that is PbI_2-like in which one-third of the metallic site are now empty (Fig. 2). Bulk BiI_3 is black powder, melts at 408 °C, sublimes at lower temperature and has an energy gap of 1.73 eV [2]. The comparison between Figs. 1b and 2b clearly shows that the BiI_3 layer is looser than PbI_2 layer, which is driven by the different positive charge of Bi^{3+} and Pb^{2+}.

2.2. Zero dimensional M/I clusters

2.2.1. Mononuclear clusters: $[BiI_6]^{3-}$, $[PbI_6]^{4-}$

The simplest iodometalates are the mononuclear clusters $[BiI_6]^{3-}$ and $[PbI_6]^{4-}$. The geometry about M atoms is a nearly ideal octahedron as shown in Fig. 3. The representative compounds are $[PhCH_2CH_2NH_3]_4[BiI_6][I]\cdot 2H_2O$ [22] and $[CH_6N]_4[PbI_6]\cdot 2H_2O$ [23]. In the former compound, the less negative charged $[BiI_6]^{3-}$ unit has to crystallize with one free I^- anion to balance the positive cations while the latter Pb-cluster needs not. One unusual mononuclear complex is $[Pr_4N]_2[PbI_4]$ [24] in which the tetrahedrally coordinated geometry about Pb atom is rare (Fig. 4).

2.2.2. Binuclear clusters $[Bi_2I_8]^{2-}$, $[Bi_2I_9]^{3-}$, $[Bi_2I_{10}]^{4-}$, $[Pb_2I_6]^{2-}$

The known compounds reveal three different motifs for dimerization of the octahedron building unit. (1) dimer of a unique five-fold-coordinate Bi as in $[(PhCH_2)_4P]_2[Bi_2I_8]$, [25] (Fig. 5) (2) dimer *via* sharing a BiI_6 octahedron face, as shown in Fig. 6, and (3) dimer *via* sharing a BiI_6 octahedron edge (Fig. 7). Example (1) suggests that the BiI_6^{3-} octahedron unit is cable of having an axial vacant of I^-. In case of (2) and (3), the geometry of BiI_6^{3-} building unit is close to the ideal octahedron, the Bi-μ_t-I (one-fold-coordinate I atom) bond (3.0 Å) is 0.2 Å shorter than the Bi-μ_2-I (two-fold-coordinate I atom) bond. The known compounds are $Cs_3Bi_2I_9$ [26,27], $[Me_4N]_3[Bi_2I_9]$ [28], $[Et_2NH_2]_3[Bi_2I_9]$ [29], and $[bpyH]_4[Bi_2I_{10}]$ [30].

However, only one Pb/I binuclear cluster is found as $[PPh_4]_2[Pb_2I_6]$ [24], in which the dimer of the four-fold coordinate

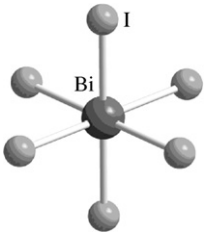

Fig. 3. Structure of mononuclear $[BiI_6]^{3-}$ [22,23].

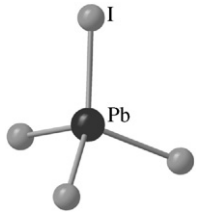

Fig. 4. Structure of mononuclear $[PbI_4]^{2-}$ [24].

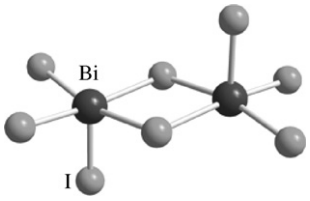

Fig. 5. Structure of binuclear $[Bi_2I_8]^{2-}$ [25].

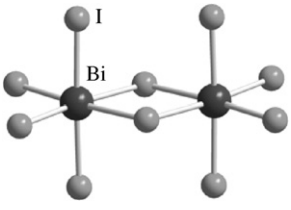

Fig. 6. Structure of binuclear $[Bi_2I_9]^{3-}$ [26–29].

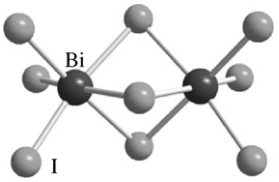

Fig. 7. Structure of binuclear $[Bi_2I_{10}]^{4-}$ [30].

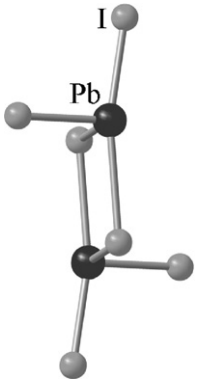

Fig. 8. Structure of binuclear $[Pb_2I_6]^{2-}$ [24].

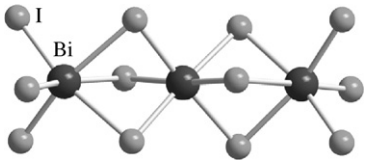

Fig. 9. Structure of trinuclear *trans* $[Bi_3I_{12}]^{3-}$ [31].

PbI_4 polyhedron is unique (Fig. 8). Note that in such a compound, the PbI_6^{4-} octahedron building unit is cable of having two equatorial sites vacant of I^- to give rise to PbI_4^{2-} species, which can also be crystallized in the compound shown in Fig. 4 [24]. However, the hypothetic BiI_4^- has never been found in a real compound, the reason may be the size of any monovalent cation is too small to crystallize with the large BiI_4^- species.

2.2.3. Trinuclear clusters $[Bi_3I_{12}]^{3-}$, $[Pb_3I_{10}]^{4-}$

Three BiI_6 octahedra can be arranged in either a *trans*-motif as $[n\text{-}Bu_4N]_3[Bi_3I_{12}]$ (Fig. 9) [31] or a *cis*-motif as $[N(CH_3)(n\text{-}C_4H_9)_3]_3[Bi_3I_{12}]$ (Fig. 10) [32]. The central octahedron therefore shares two opposite or cis I–I–I faces. The *trans*-$[Bi_3I_{12}]^{3-}$ cluster possesses C_{3v} symmetry with three Bi atoms on a threefold axis. Such an assembly could also be seen as a combination of a binuclear $[Bi_2I_9]^{3-}$ and an additional BiI_6^{3-} octahedron.

On the other hand, the trinuclear $[Bu_3N(CH_2)_4NBu_3]_2[Pb_3I_{10}]$ [13] complex possesses a closed loop motif of two normally 6-fold coordinate PbI_6 octahedra and one unusual PbI_5 square-pyramid (Fig. 11). If a trinuclear Pb-cluster used the same motif as for the Bi-analogue shown in Fig. 9, the resultant species would be $Pb_3I_{12}^{6-}$, which carries too much negative charge, and thus would be unstable.

The variation of the coordination number (CN) of MI_x (x = 6, 5, 4) also indicates the considerable tolerance of MI_6 octahedron to endure the distortion. Such tolerance arises from the flexibility of the central Bi or Pb ions and the less direction-correlation nature of the covalent M–I bonds. The size and charge of the MI_x polyhedron are also important factors to determine its stability.

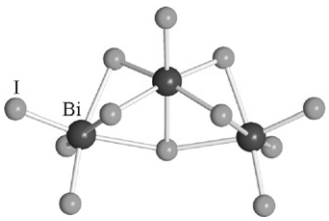

Fig. 10. Structure of trinuclear *cis* $[Bi_3I_{12}]^{3-}$ [32].

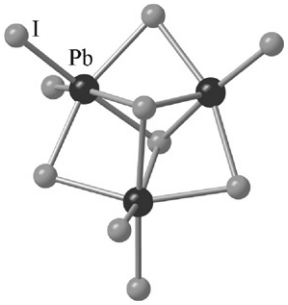

Fig. 11. Structure of trinuclear closed $[Pb_3I_{10}]^{4-}$ [13].

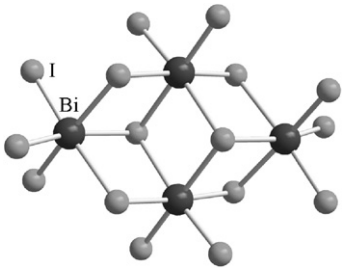

Fig. 12. The structure of tetranuclear $[Bi_4I_{16}]^{4-}$ [13,33].

2.2.4. Tetranuclear cluster $[Bi_4I_{16}]^{4-}$

The tetranuclear $[Bi_4I_{16}]^{4-}$ cluster (Fig. 12), is a dimer of a binuclear $[Bi_2I_{10}]^{4-}$(Fig. 7) *via* two common μ_2- and two μ_3-I atoms. Compared with the binuclear species, no obvious changes in Bi–I bond distances or I–Bi–I angles are found. Two examples are compounds $[BiPc]_4[Bi_4I_{16}]$ and $[C_3H_9COSC_2H_4N(CH_3)_3]_4[Bi_4I_{16}]$ [33,34].

2.2.5. Pentanuclear clusters $[Bi_5I_{18}]^{3-}$, $[Bi_5I_{19}]^{4-}$, $[Pb_5I_{16}]^{6-}$

Five BiI_6^{3-} octahedra could be arranged linearly as found in $[Ph_4P]_3[Bi_5I_{18}]$ [35] and $[Ph_4Sb]_3[Bi_5I_{18}]$ [36] shown in Fig. 13. Such pentanuclear clusters can be viewed as a combination of a binuclear $[Bi_2I_9]^{3-}$ (Fig. 6) and a trinuclear $[Bi_3I_{12}]^{3-}$ (Fig. 9) *via* a shared I–I–I face. This illustrates that the μ_t-I atoms in some small clusters is still coordination active. Interestingly, a different aggregation pattern of five BiI_6 octahedra is found in $[Li(THF)_4]_4[Bi_5I_{19}]$ [37], which is a combination of a tetranuclear $[Bi_4I_{16}]^{4-}$ (Fig. 12) and a $[BiI_6]^{3-}$ octahedron through one μ_3-I and two μ_2-I atoms (Fig. 14).

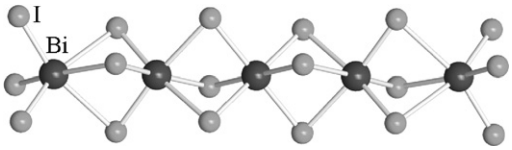

Fig. 13. Structure of pentanuclear $[Bi_5I_{18}]^{3-}$ [35,36].

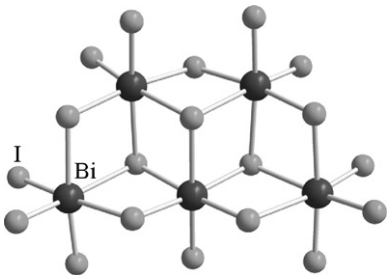

Fig. 14. Structure of pentanuclear $[Bi_5I_{19}]^{4-}$ [38].

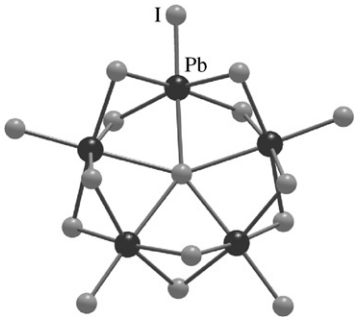

Fig. 15. Structure of pentanuclear $[Pb_5I_{16}]^{6-}$ [24].

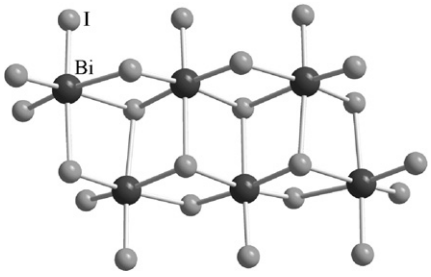

Fig. 16. Structure of type-I hexanuclear $[Bi_6I_{22}]^{4-}$ [37–39].

In a third fashion, five PbI_6 octahedra are arranged in a close loop, a higher symmetric motif as shown in Fig. 15, in which the occurrence of an unusual μ_5-I is crucial for the structure, and the five Pb atoms are almost coplanar. The example is found in $[BuN(CH_2CH_2)_3NBu]_3[Pb_5I_{16}]\cdot 4DMF$ [24]. A similar closed motif occurs in the trinuclear cluster discussed above.

2.2.6. Hexanuclear clusters $[Bi_6I_{22}]^{4-}$

No hexanuclear Pb/I cluster has been found so far. On the contrary, six BiI_6^{3-} octahedron can be arranged in three different hexanuclear patterns. The planar type-I (Fig. 16) exists in $[Ph_4P]_4[Bi_6I_{22}]$, $[Na(THF)_6]_4[Bi_6I_{22}]$ [37], $[Et_4P]_4[Bi_6I_{22}]$ [38], and $[PhEt(Me)_2N]_4[Bi_6I_{22}]$ [39]. Type-II, $[PhCH_2NEt_3]_4[Bi_6I_{22}]$ [35], has no planarity (Fig. 17). An unusual μ_4-I atom in type-III (Fig. 18) occurred in $[Ru(C_{10}H_8N_2)_3]_2[Bi_6I_{22}]$ [40]. If the same hexanuclear Pb-cluster existed, the negative charges of such a hypothetical Pb_6I_{22} would be −10, which is too high to find any suitable compensation cation.

2.2.7. Heptanuclear cluster $[Pb_7I_{22}]^{8-}$

$[Bu_3N(CH_2)_4NBu_3]_4[Pb_7I_{22}]$ [13] (Fig. 19) is the only known heptanuclear cluster, and there is none for Bi/I. At first sight, such a cluster would be impossible, but it is quite reasonable because it can be viewed as two trinuclear $[Pb_3I_{10}]^{-}$ (Fig. 11) connected by a

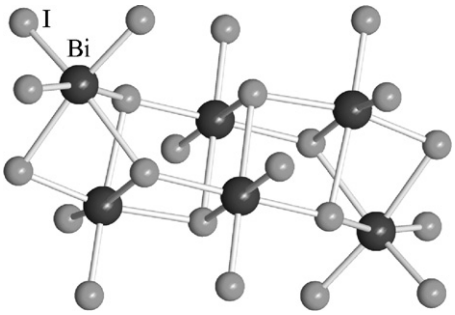

Fig. 17. Structure of type-II hexanuclear $[Bi_6I_{22}]^{4-}$ [35].

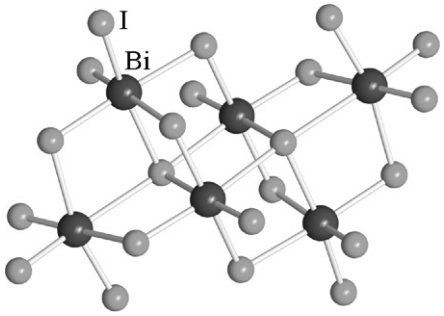

Fig. 18. Structure of type-III hexanuclear $[Bi_6I_{22}]^{4-}$ [40].

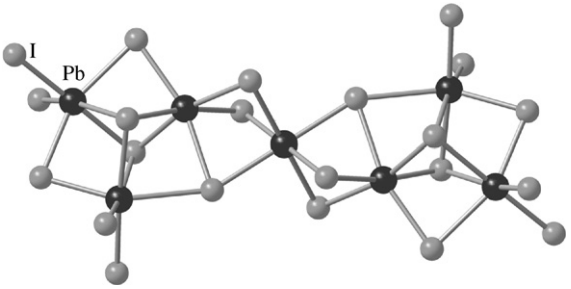

Fig. 19. Structure of heptanuclear $[Pb_7I_{22}]^{8-}$ [13].

PbI_6^{4-} octahedron *via* shared opposite I–I–I faces. Such an example also illustrates the stability of the unusual $[Pb_3I_{10}]^{4-}$.

2.2.8. Octanuclear clusters $[Bi_8I_{28}]^{4-}$, $[Bi_8I_{30}]^{6-}$

Two ways to construct the structure of octanuclear $[Bi_8I_{28}]^{4-}$ (Fig. 20) are (1) a [6+2] addition complex of a hexanuclear $[Bi_6I_{22}]^{4-}$ (Fig. 16) and two BiI_6 octahedra as occurred in $[Ph_4P]_4[Bi_8I_{28}]$ [41] and (2) the conceptual [4+4] dimerization of the tetranuclear cluster as found in compound $[Bi_3I(C_4H_8O_3H_2)_2(C_4H_8O_3H)_5]_2[Bi_8I_{30}]$ (Fig. 21) [42]. These two examples suggest that, beyond the mononuclear BiI_6 octahedron, some other small multinuclear clusters can also serve as building units to construct larger polynuclear clusters.

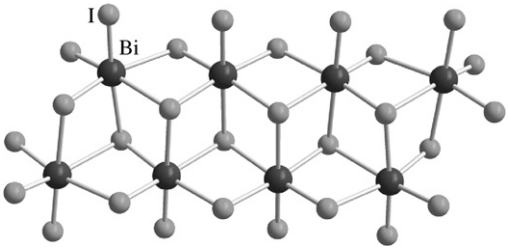

Fig. 20. Structure of octanuclear $[Bi_8I_{28}]^{4-}$ [41].

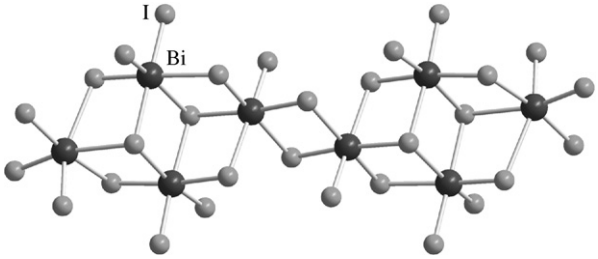

Fig. 21. Structure of octanuclear $[Bi_8I_{30}]^{6-}$ [42].

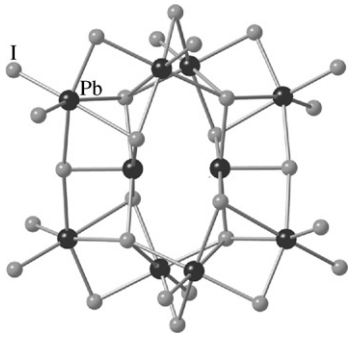

Fig. 22. Structure of $[Pb_{10}I_{28}]^{8-}$ [32].

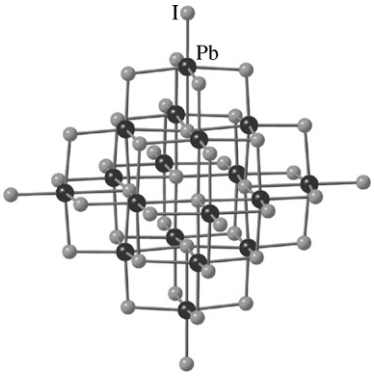

Fig. 23. Structure of $[Pb_{18}I_{44}]^{8-}$ [11].

2.2.9. Decanuclear and octadecanuclear clusters $[Pb_{10}I_{28}]^{8-}$, $[Pb_{18}I_{44}]^{8-}$

$[Pb_{10}I_{28}{}^{8-}]$ (Fig. 22) [13], and $[Pb_{18}I_{44}{}^{8-}]$ (Fig. 23) [11] are two crystalline examples constructed by more than ten metal centers in which the geometry of the PbI_6 octahedron is well conserved.

In contrast to 0D Pb/I clusters, Bi/I species tend to aggregate more into discrete polynuclear clusters. The essential reason is that for a certain number of metal centers, the Bi-cluster carries a higher positive charge which allows more terminal I atoms to "protect" the discrete cluster and prevent the extension of the building unit.

2.3. One-dimensional M/I polymeric chains

1D polymeric chains, common in iodometalates, are built from basic MI_6 octahedron or relatively larger units, such as Pb_3I_{10} or Bi_4I_{14}, *via* different connection motifs.

2.3.1. Linear chains constructed by mononuclear cluster $[BiI_6]^{3-}$ or $[PbI_6]^{4-}$

2.3.1.1. Via shared faces. The most common chain motif for iodoplumbates is found in [17,20] by the infinite connection of PbI_6 octahedron via shared I–I–I faces (Fig. 24). The octahedron (O) of PbI_6 can be deformed to a large degree to trigonal prism (TP) in complex 1,1′-dimethyl-4,4′bipyridinium (Fig. 25) [43].

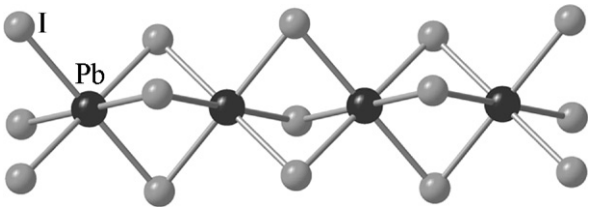

Fig. 24. Structure of $[PbI_3{}^-]_n$ [17,20].

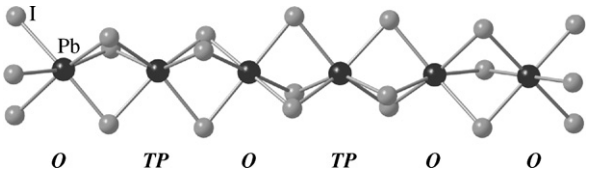

Fig. 25. Structure of $[Pb_6I_{18}{}^{6-}]_n$ [43].

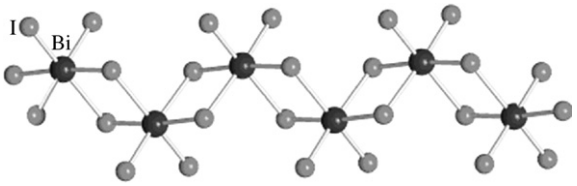

Fig. 26. Structure of $[BiI_4{}^-]_n$ [30,44–46].

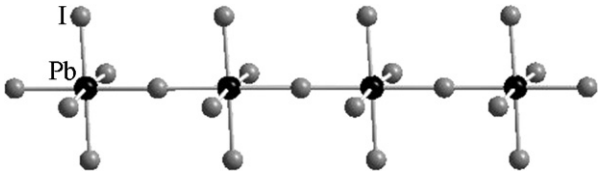

Fig. 27. Structure of anionic chain in $[NH_2C(I){=}NH_2]_{3n}[PbI_5]_n$ [47].

2.3.1.2. Via shared edges. Compounds [biPyH][BiI_4], [30] [C_9H_8N][BiI_4], [44] [$(C_2H_4N_3S)(C_2H_3N_3S)$[BiI_4] [45] and $NH_3(CH_2)_2NH_3(BiI_4)_2{\cdot}4H_2O$ [46] are examples in which BiI_6 octahedra that share edges constitute a linear chain (Fig. 26).

2.3.1.3. Via shared apexes. The PbI_6 octahedron may share cis or trans apexes to give $[NH_2C(I){=}NH_2]_{3n}[PbI_5]_n$ [47], as shown in Fig. 27 or $[C_6H_5CH_2CH_2S{=}C(NH_2)_2]_{3n}[PbI_5]_n$ [48], Fig. 28. This pattern is also adopted by BiI_6 octahedra in $[H_3N(CH_2)_6NH_3][BiI_5]_n$ (Fig. 29) [49]. In both structures, the metal atoms are coplanar.

2.3.2. Linear chains constructed by binuclear $[Pb_2I_6]^{2-}$, trinuclear cluster $[Pb_3I_{10}]^{4-}$ or tetranuclear $[Bi_4I_{14}]^{2-}$

Except for the $MI_6{}^{n-}$ octahedron, some polynuclear clusters can also serve as conceptual building units, such as binuclear $[Pb_2I_9]^{5-}$ unit in $[M(en)_3]_n[Pb_2I_6]_n$ (M = Mn, Fe, Zn, Ni; en = ethylenediamine) (Fig. 30) [50]; trinuclear $[Pb_3I_{10}]^{4-}$ units

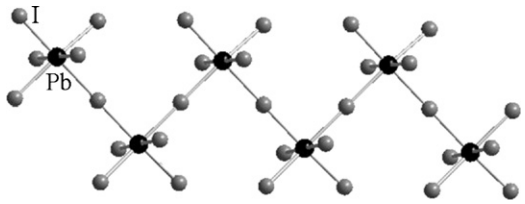

Fig. 28. Structure of anionic chain in $[C_6H_5CH_2CH_2S{=}C(NH_2)_2]_{3n}[PbI_5]_n$ [48].

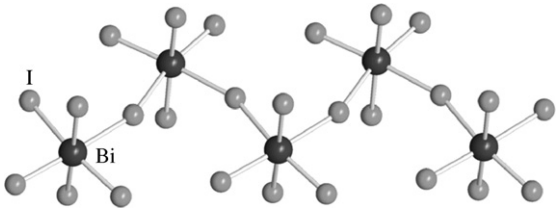

Fig. 29. Structure of anionic chain in $[H_3N(CH_2)_6NH_3]_n[BiI_5]_n$ [49].

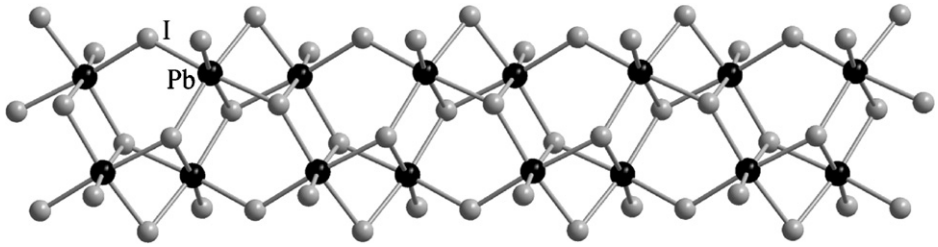

Fig. 30. Structure of anionic chain in $[M(en)_3]_n[Pb_2I_6]_n$ [50].

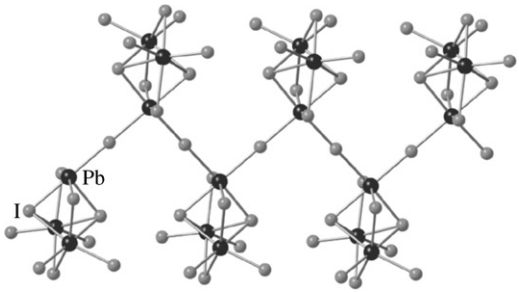

Fig. 31. Structure of anionic chain in $[Me_3N(CH_2)_2NMe_3]_{2n}[Pb_3I_{10}]_n$ [51].

in $[Me_3N(CH_2)_2NMe_3]_{2n}[Pb_3I_{10}]_n$ (Fig. 31) [51] and tetranuclear $[Bi_4I_{14}]^{2-}$ units in $[n\text{-}Bu_4N]_{2n}[Bi_4I_{14}]_n$ [29], or $[CH_2{=}C(C_6H_4\text{-}4\text{-}NO_2)CH_2NMe_3]_{2n}[Bi_4I_{14}]_n$ (Fig. 32) [34]. In another case, the tetranuclear building units are linked by binuclear $[Bi_2I_8]^{2-}$ in $[Et_3PhN]_{4n}[Bi_6I_{22}]_n$ (Fig. 33) [41].

2.3.3. *Wider chains*

Most of the chains described above are of a single string of MI_6 octahedra but there are some wider chains formed by several strings of MI_6 octahedra as follows.

In $[C_{10}H_7CH_2NH_3]_n[PbI_3]_n$ [48], the anionic chains are two condensed linear PbI_6 chains that share octahedron edges (Fig. 34). In another case, the anionic chain in $[PPh_4]_{2n}[Pb_5I_{12}]_n$ [13] is made up of two PbI_6 strings together with some individual PbI_6 octahedra (Fig. 35).Additionally, three strings of MI_6 octahedra form the

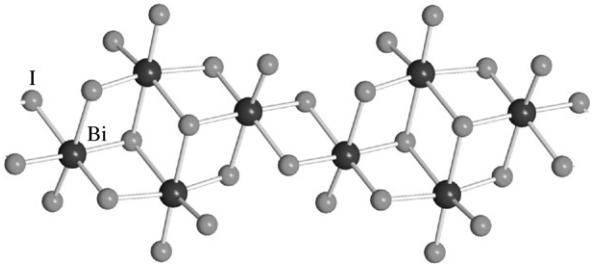

Fig. 32. Structure of $[Bi_4I_{14}{}^{2-}]_n$ [29,34].

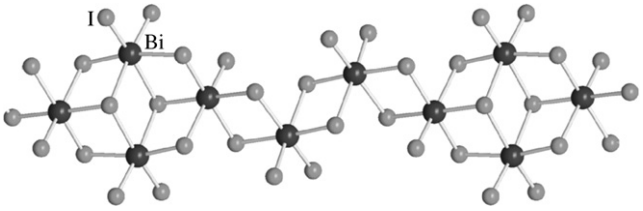

Fig. 33. Structure of anionic chain in $[Et_3PhN]_{4n}[Bi_6I_{22}]_n$ [41].

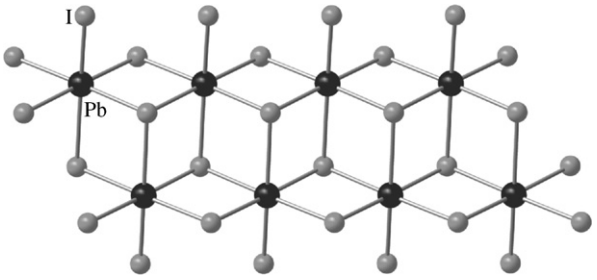

Fig. 34. Structure of $[PbI_3{}^-]_n$ [48].

anionic chain in $[PPh_4]_{2n}[Pb_6I_{14}(DMF)_2]_n$ [52] as shown in Fig. 36, in which half of the peripheral Pb-octahedra have a coordination sphere of five I atoms and one DMF solvent molecule. Interestingly, the middle string of PbI_6 octahedra is reminiscent of those in PbI_2 binary. Furthermore, an anionic chain of six strings of MI_6 octahedra exists in $[M_4(2,2'\text{-bipy})_{12}Pb_{11}I_{28}S]_n$ (M = Ni, Co) [53], as shown in Fig. 37. Again, the inner Pb atoms that are surrounded by six neighboring Pb atoms have the same motif as that in binary PbI_2.

If the number of strings of MI_6 octahedra would reach infinity, the anionic structure would be a 2D layer. However, experimental data illustrating such a stepwise development are still lacking.

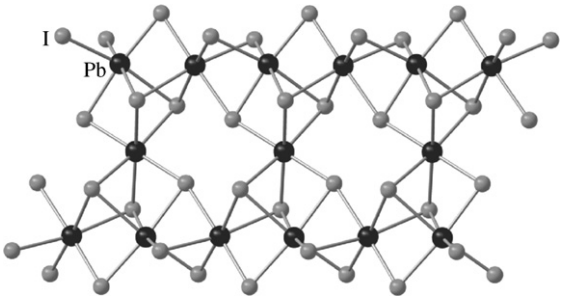

Fig. 35. Structure of $[Pb_5I_{12}{}^{2-}]_n$ [13].

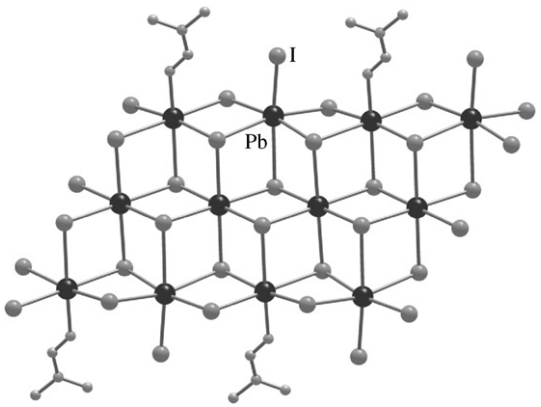

Fig. 36. Structure of $[Pb_6I_{14}(DMF)_2{}^{2-}]_n$ [52].

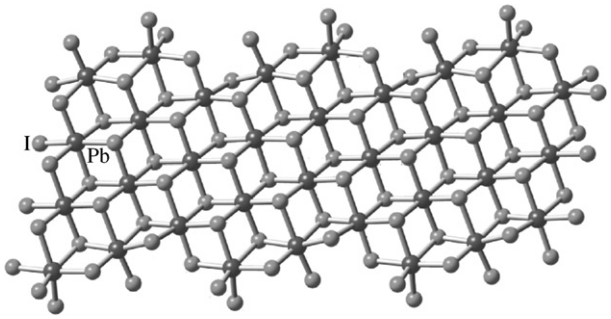

Fig. 37. Structure of $[Pb_{11}I_{28}S^{8-}]_n$ [53].

2.4. Two-dimensional polymeric M/I layer

The majority of the M/I layers are of perovskite-type construction. A different number of layers (m) in the 3D perovskite network could be separated by different organic cations to give the 2D layered compounds. The simplest example of this family is $(CH_3C_6H_4CH_2NH_3)_2PbI_4$ [48,54–57], in which each layer of PbI_6 octahedra is separated by organoammonium cations $(CH_3C_6H_4CH_2NH_3)^+$ (Fig. 38).

A double PbI_6 layer crystallizes with a small cation $(CH_3NH_3)^+$ to fit inside the inorganic layer (Fig. 39).

Studies have shown that the number (n) of single perovskite type PbI_6-layers can be 1, 2, 3, 4, 5, and ∞, in the $(RNH_3)_2(CH_3NH_3)_{n-1}M_nX_{3n+1}$ family, (M = Pb, Sn and Cu, X = Cl, Br, I, and R = C_4H_9, $C_6H_5C_2H_4$) [58–60]. The compound $(H_2AEQT)Bi_{2/3}I_4$ [61] also adopts a perovskite type structure in which the Bi/I layer is a single perovskite layer. Also a new staircase-like 2D $[Pb_4I_{18}{}^{10-}]_n$ sheet of perovskite type is crystallized with the co-template organic anions $(C_2O_4)^{2-}$ and organic cations $(H_2en)^{2+}$ [62].

Besides the perovskite-type connections, there are some other patterns found in layered iodometalates. One newly synthesized $[Pb_4I_{10}{}^{2-}]_n$ anionic layer (Fig. 40) [63] is the most condensed anionic layered iodoplumbate, in which the connection of $PbI_6{}^{4-}$ octahedron is comparable to that in a binary PbI_2 sheet but of lower symmetry. The other known layered iodometalates are constructed with polynuclear building units instead of the mononuclear MI_6 octahedron, for example, binuclear $[Pb_2I_7]^{3-}$ in $[Me_3NC_2H_4NMe_3]_2[Pb_2I_7]I$ [64] (Fig. 41), trinuclear $[Pb_3I_{10}{}^{4-}]_n$ in $[C_5H_6CH_2SC(NH_2)_2]_4[Pb_3I_{10}]$ (Fig. 42), or hexanuclear $[Pb_6I_{18}]^{6-}$ in $[Me_3NC_3H_6NMe_3]_3[Pb_6I_{18}]$ (Fig. 43) [51].

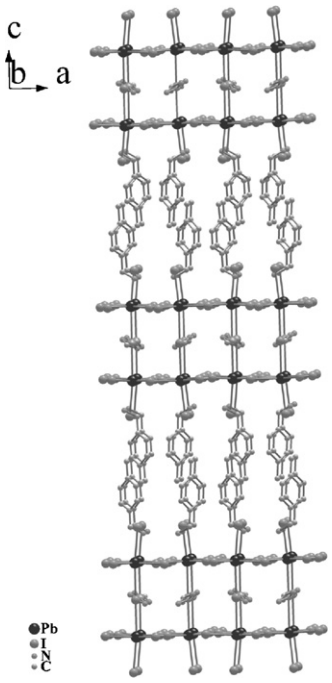

Fig. 39. Structure of $[(CH_3C_6H_4CH_2NH_3)_2(CH_3NH_3)]_n[Pb_2I_7]_n$, and $[Pb_2I_7{}^{3-}]$ layer with double connected perovskite type PbI_6 layers accommodating small $(CH_3NH_3)^+$ cations [58–60].

2.5. Three-dimensional polymeric Pb/I network

Only one example of 3D Pb/I inorganic framework is found in compound $[EDAMP]_{2n}[Pb_7I_{18}]_n{\cdot}4nH_2O$ (EDAMP = $Et_2NHC_6H_4CH_2C_6H_4NHEt_2$) (Fig. 44) [65].

The PbI_6 octahedra generate the wall of the 3D inorganic open-framework structure with a $CdSO_4$-type topology. Within such a network, the tunnel accommodates the EDAMP ions and lattice water molecules. The packing density of this compound is very loose; the guest molecule occupies about 45.0% of the crystal volume.

2.6. A brief structure summary

All the iodometalate anions described above show that there are two structural types of I atoms, terminal (μ_t-I, $t = 1$) and bridging

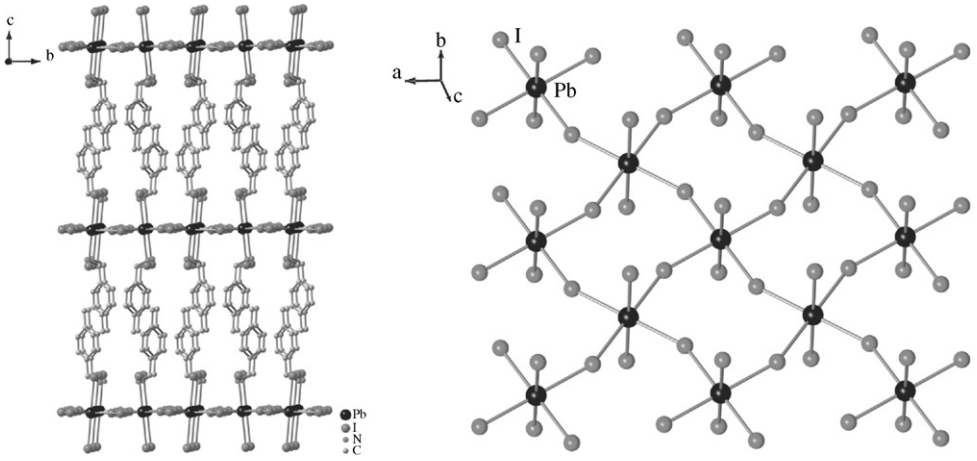

Fig. 38. (a) Structure of $[CH_3C_6H_4CH_2NH_3]_{2n}[PbI_4]_n$ [48,54–57], and (b) a single perovskite type PbI_6-layer.

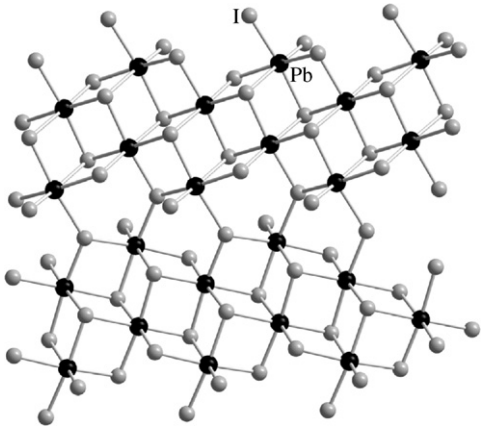

Fig. 40. Structure of $[Pb_4I_{10}^{2-}]_n$ anionic layer [63].

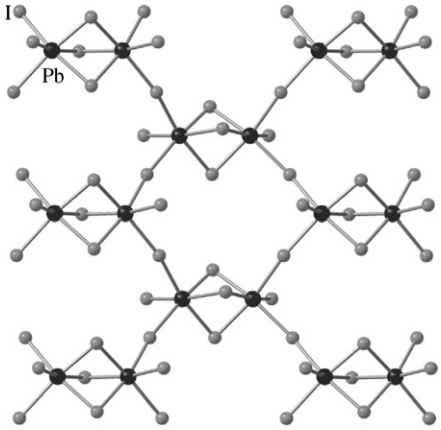

Fig. 41. Structure of $[Pb_2I_7^{3-}]_n$ anionic layer [64].

iodine (μ_n-I, n = 2–6). The μ_t-I (one-fold-coordinate iodine atom) functions as a peripheral atom, which serves to isolate the M/I cluster (i.e., to terminate the polymerization of the building units). The μ_n-I (n-fold-coordinate iodine atom) is responsible for the aggregation and polymerization of MI_6 octahedra.

The major structural difference between iodobismuthate and iodoplumbate originates from the charge difference. For example, in case of the neutral binary compound, Bi^{3+} cation which carries a higher positive charge, requires a lower Bi:I ratio of 1:3 (Bi^{3+}:3I^-) than Pb^{2+} does (Pb^{2+}:2I^- = 1:2). Although the building units in these

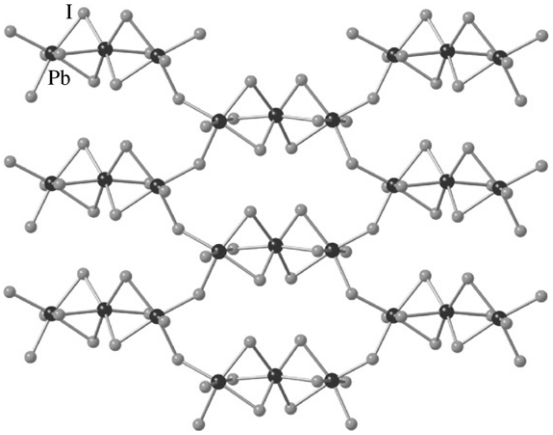

Fig. 42. Structure of $[Pb_3I_{10}^{4-}]_n$ anionic layer [51].

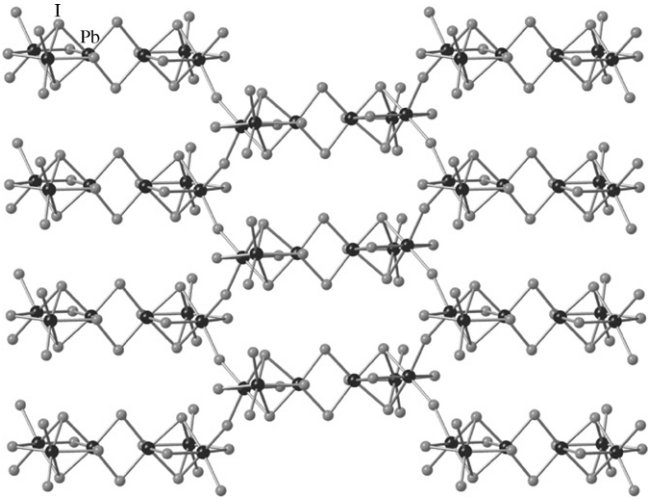

Fig. 43. Structure of $[Pb_6I_{18}^{6-}]_n$ anionic layer [51].

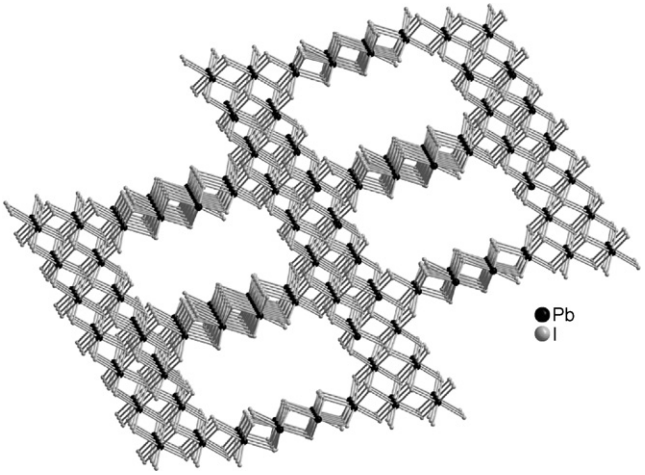

Fig. 44. Structure of 3D $[Pb_7I_{18}^{4-}]_n$ anionic 3D open framework [65].

two compounds are similar MI_6 octahedra, the BiI_3 binary with a higher I content requires a relatively larger number of lower coordinated I^- anions and then crystallizes in a looser structure, that is a PbI_2-like structure with one-third of the metallic site vacancy. On the other hand, in the case of anionic iodometalates, the PbI_6^{4-} unit that carries more negative charge with respect to the BiI_6^{3-} octahedron, is likely to form relatively more condensed structures in order to reduce the total number of iodine ions and to keep the anionic charge density as low as possible. In addition, such a charge-driven characteristic leads to the fact that the iodobismuthate anion tends to form simple clusters with low nuclearity or polymers with low dimensionality, while the iodoplumbate tends to form polynuclear clusters or polymers with higher dimensionalities. As described above, the number of 0D iodobismuthate clusters is greater than that of iodoplumbate, but 2D or 3D structures are only found in iodoplumbate system.

3. An experimental structure–property indicator *M*/*r* value

The structure of the inorganic anionic moiety determines most of the properties of iodoplumbates and iodobismuthates. We have so far summarized the majority structural types of their inorganic moieties. The structural changes are somewhat associated with the aggregation of the primary unit of MI_6 octahedron. The aggregation density of the inorganic moiety (ADIM) is an important structural

parameter that is related to the physical properties. From the point view of electronic structure, the fluctuation of the bands reflects the interaction intensity of the orbitals. The more condensed the building unit aggregates, the stronger and larger the orbital interactions are, and thus the more fluctuant the bands are, which will directly influence the band gap and the electronic density.

Meanwhile, several structural parameters may be related to ADIM, such as (a) density of the single crystal (ρ), (b) nuclearity of the inorganic moiety, i.e. the number of metal centers of a discrete cluster, or (c) dimension of the inorganic part. But none of them can conveniently and quantifiably express ADIM. For example, ρ is an overall density including the contribution of the organic cations, and therefore is not merely determined by ADIM. The nuclearity can somehow qualitatively indicate the aggregation of a discrete cluster, i.e., the higher the nuclearity the higher the densities of the clusters. But there are many exceptions. Thus both $[Bi_8I_{28}]^{4-}$ (Fig. 20) and $[Bi_8I_{30}]^{6-}$ (Fig. 21) have eight Bi centers, but the density of the latter is lower. The dimensionality is also weak in this respect. For example, the dimension of $[PbI_3^-]_n$ (Fig. 24) is 1D, higher than that of 0D polynuclear $[Pb_{18}I_{44}]^{8-}$ (Fig. 23), but clearly, the ADIM of the octadecanuclear cluster is much higher. Besides, 1D anionic chains can be either linear chain, or fatter chains, or chains constructed by complicated building units and their ADIM are very different.

Therefore, if a structure parameter could indicate ADIM, it would be helpful to directly relate the structural characteristic with the physical property. We found that the type of μ_n-I is a key to understand the structure of iodoplumbate and iodobismuthate. For instance, μ_t-I terminates extension of the building block, so that the more μ_t-I atoms a cluster wears, the less possibility for such cluster to polymerize. The μ_2-I atoms correspond to the bridging of two neighboring octahedra, and μ_3-I, aggregation of three octahedra, and so on. Therefore we have defined an r value as $r = \Sigma(N\mu_n\text{-I})/n$, $N\mu_n$-I means the number of μ_n-I (n-fold-coordinate I) atoms per building unit and n = 1–6; and the M/r value as $M/r = M{:}r$ (M = the number of metal centers per building unit), which empirically indicates ADIM. Some representative iodometalates, their structural features, and the corresponding r and M/r values are listed in Table 1.

Naturally, binary PbI_2 is the most condensed Pb/I compound and any introduction of cations into Pb/I system will put negative charges on the inorganic moiety and thus decrease ADIM, therefore, the M/r upper limit in the Pb/I iodoplumbate is 1.5. Similarly, the M/r maximum is 0.67 of binary BiI_3 for the Bi/I system. The structural description above show that BiI_3 is less condensed than PbI_2 since it is a derivative of a PbI_2-type structure with 1/3 vacancy; coherently, the M/r ratio of BiI_3 (0.67) is less than that of PbI_2 (1.5), such a reduction in M/r is consistent with the decrease of ADIM. The M/r ratio of 0D cluster also monotonously decreases with the decrease of the nuclearity of a cluster. As listed in Table 1, each series of 0D iodoplumbate or iodobismuthate clusters, clearly shows that the higher the number of metal centers, the higher the density of a discrete cluster, the larger the M/r ratio. For example, the M/r ratios increase from 0.4 of $[Pb_2I_6]^{2-}$ to 0.82 of $[Pb_{18}I_{44}]^{8-}$. The increase of the M/r ratio also agrees with the increase of dimensionality. For example, three complexes constructed from the same building unit have a nice conceptional dimensional development from 0D $[Pb_3I_{10}]^{4-}$ cluster (Fig. 11) to 1D $[Pb_3I_{10}{}^{4-}]_n$ chain (Fig. 31), and to 2D $[Pb_3I_{10}{}^{4-}]_n$ layer (Fig. 42). Their densities increase as the dimension increases and their M/r ratio, increases monotonously from 0.42 to 0.45 to 0.50. Note that only comparisons within polymers that are made by the same building unit have a direct relevance to the development of the dimensionality since several other factors also affect the density of 1D or 2D polymers, such as the type of building unit, the extension motif, and so on.

Table 1
Representative iodoplumbates, iodobismuthates and their r and M/r values.

M	Compound	Structure	$r = \Sigma(N\mu_n\text{-I})/n$	M/r ratio	E_g
Pb	PbI_2	Fig. 1	2/3 = 0.67	1.5	
	$[Pb_{18}I_{44}]^{8-}$	Fig. 23	6 + 24/2 + 8/3 + 6/5 = 21.87	0.82	
	$[Pb_{10}I_{28}]^{8-}$	Fig. 22	12 + 6/2 + 6/3 + 4/4 = 18	0.56	
0D	$[Pb_7I_{22}]^{8-}$	Fig. 19	8 + 8/2 + 6/3 = 14	0.5	
	$[Pb_5I_{16}]^{6-}$	Fig. 15	5 + 10/2 + 1/5 = 10.2	0.49	
	$[Pb_3I_{10}]^{4-}$	Fig. 11	5 + 3/2 + 2/3 = 7.17	0.42	
	$[Pb_2I_6]^{2-}$	Fig. 8	4 + 2/2 = 5	0.4	
1D	$[Pb_5I_{12}{}^{2-}]_n$	Fig. 34	6/3 + 6/2 = 5	1	
	$[Pb_6I_{18}{}^{6-}]_n$	Fig. 25	18/2 = 9	0.66	
	$[PbI_3^-]_n$	Fig. 24	3/2	0.66	
	$[Pb_3I_{10}{}^{4-}]_n$	Fig. 31	4 + 4/2 + 2/3 = 6.67	0.45	
	$[PbI_5{}^{3-}]_n$	Fig. 28	4 + 1/2 = 4.5	0.22	
2D	$[Pb_3I_{10}{}^{4-}]_n$	Fig. 42	2 + 8/2 = 6	0.5	
	$[Pb_2I_7{}^{3-}]_n$	Fig. 14	2 + 5/2 = 4.5	0.44	
	$[PbI_4{}^{2-}]_n$	Fig. 38	2 + 2/2 = 3	0.33	
Bi	BiI_3	Fig. 2	3/2 = 1.5	0.67	1.73
	$[Bi_5I_{18}]^{3-}$	Fig. 13	6 + 12/2 = 12	0.42	
	$[Bi_8I_{28}]^{4-}$	Fig. 20	14 + 8/2 + 6/3 = 20	0.4	
	$[Bi_6I_{22}]^{4-}$	Fig. 16	12 + 6/2 + 4/3 = 16.33	0.37	
	$[Bi_8I_{30}]^{6-}$	Fig. 21	16 + 10/2 + 4/3 = 22.33	0.36	
	$[Bi_5I_{19}]^{4-}$	Fig. 14	11 + 5/2 + 3/3 = 14.5	0.344	
0D	$[Bi_4I_{16}]^{4-}$	Fig. 12	10 + 4/2 + 2/3 = 12.667	0.32	2.16
	$[Bi_3I_{12}]^{3-}$	Fig. 9	6 + 6/2 = 9	0.33	
		Fig. 10	7 + 4/2 + 1/3 = 9.33	0.32	
	$[Bi_2I_8]^{2-}$	Fig. 5	6 + 2/2 = 7	0.29	2.19
	$[Bi_2I_9]^{3-}$	Fig. 6	6 + 3/2 = 7.5	0.27	
	$[Bi_2I_{10}]^{4-}$	Fig. 7	8 + 2/2 = 9	0.22	
	$[BiI_6]^{2-}$	Fig. 3	6	0.17	
1D	$[Bi_4I_{14}{}^{2-}]_n$	Fig. 32	6 + 6/2 + 2/3 = 9.67	0.41	2.02
	$[Bi_6I_{22}{}^{4-}]_n$	Fig. 33	10 + 10/2 + 2/3 = 15.67	0.38	
	$[BiI_4^-]_n$	Fig. 26	2 + 2/2 = 3	0.33	
	$[BiI_5^-]_n$	Fig. 29	4 + 1/2 = 4.5	0.22	

More significantly, the M/r ratio decreases with the increase of the energy gap, as listed in Table 1. The M/r ratios for BiI_3 (2D), $[Bi_4I_{14}{}^{2-}]$ (1D), $[Bi_4I_{16}]^{2-}$ (0D), and $[Bi_2I_9]^{2-}$ (0D) decrease from 0.67 to 0.41, 0.32 and 0.27 as the energy gaps increase from 1.73 to 2.02, 2.16 and 2.19 eV [66]. Such a tendency has also been found in the heterometallic Bi/M/I (M = Cu, Ag) complexes, which will be discussed in Section 5. Such a trend agrees with the general acceptance that the higher density usually measures a smaller energy gap. Hence, the structural factor M/r might be the best empirical parameter to predict the energy gaps of iodometalates with the same metal identity that is the energy gap decreases with increase of M/r. We consider such an empirical relationship might be suitable for other systems, such as Sn/I, M/X (M = Pb, Bi, Sn, X = F, Cl, Br, I or M = transition metal, X = S, Se, Te), etc. However, the available experimental data are insufficient to date, and such a rule of thumb needs to be tested.

4. Structural modification

4.1. Cation effect

The cation effect is to balance the negative charge density on the inorganic moiety so as to modify the anionic structure. Meanwhile, the simultaneous steric effect of the cation governed by its size is also important to influence modification of the anionic structure. Such effects are widely reported in iodoplumbates and iodobismuthates.

The introduction of a low charge density complex cation $[Ni(opd)_2(acn)_2]^{2+}$ (opd = o-phenylenediamine, acn = acetonitrile) can generates a novel infinite 2D $[Pb_4I_{10}{}^{2-}]_n$ anionic layer (Fig. 45b) [63] that is comparable to the hexagonal PbI_2 sheet (Fig. 45a) but in

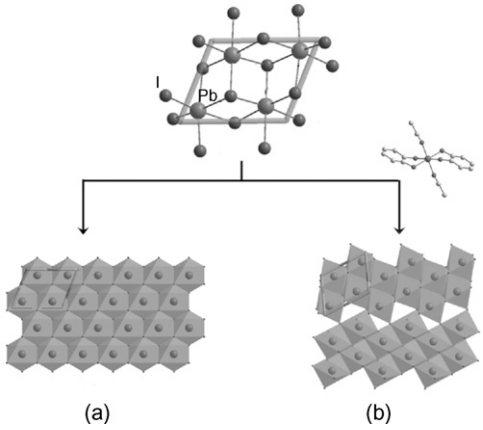

Fig. 45. Cation effect leads to the symmetry breaking. (a) Single hcp layer in PbI_2 and (b) single $[Pb_4I_{10}{}^{2-}]_n$ anionic layer, the rhombus confines the 2×2 subunit. Adapted from [63], with permission from the American Chemical Society.

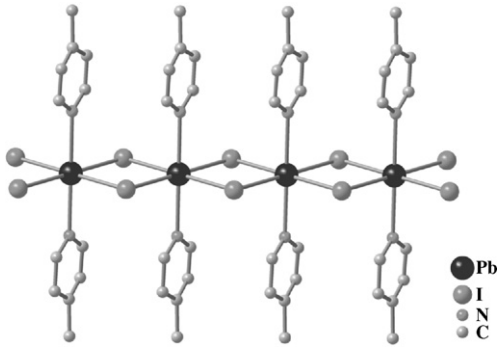

Fig. 47. Structure of $[PbI_2(4\text{-MPD})_2]_n$ [68].

a lower symmetry. The anionic layer is constructed by a 2×2 subunit $[Pb_4I_{10}]^{2-}$, and binary PbI_2 is formed by a similar 2×2 subunit with slightly different formula: $[Pb_4I_8]^0$. Two more I^- anions per subunit are involved in $[Pb_4I_{10}{}^{2-}]_n$ [63], because of the occurrence of the less coordinated μ_t-I and μ_2-I, while the I^- anions in PbI_2 are all μ_3-I. The μ_t- and μ_2-I atoms are responsible for the loose packing of PbI_6 octahedra and the extra charges are gathered on the anionic layer to balance the charge requirement of the cations.

As the cation size decreases, the dimension of the compound increases. Fig. 46 shows a nice stepwise modification of the anionic structure from a 0D cluster to a linear polymer to a ladder-like chain with a more-or-less gradual decrease of the cation size [67].

As the cation size decreases, the nuclearity of the 0D cluster decreases. For example, the cation size decreases from $[n\text{-}Bu_4N]^+$ to $[Pr_4N]^+$, the cluster decreases from an octadecanuclear $[Pb_{18}I_{44}]^{8-}$ to a mononuclear $[PbI_4]^{2-}$. From short $[NH_2C(I){=}NH_2]^+$ cation to long $[C_6H_5(CH_2)_2S{=}C(NH_2)_2]^+$ cations, the anionic moiety changes from a linear $[PbI_5{}^{3-}]_n$ chain (Fig. 27) to a wavy chain, or a zigzag chain (Fig. 28).

As the charge of the cations increase, the dimension decreases. For monovalent cations, $[C_6H_5CH_2SC(NH_2)_2]^+$ or $[(C_4S)_2SC_2H_4NH_3]^+$, the anionic moiety adopts a $[Pb_3I_{10}{}^{4-}]_n$ 2D layered structure (Fig. 42). For bivalent cations, $[Me_3N(CH_2)_2NMe_3]^{2+}$, the anionic structure is a zigzag chain motif as shown in Fig. 31.

A thoughtful choice of the size, charge, and flexibility of a cation might reward a successful synthesis of a desired compound. Of course, the crystallization of a new compound is complicated, during which many other factors, such as solvent, temperature, competition reactions, and so on, may bring unpredictable results.

4.2. Ligand effect

One direct structural change in a MI_6 building unit is to replace some of the I atoms with organic ligands, such as S-, O-, and N-ligands, which can also participate in the construction of the inorganic–organic hybrid skeleton. For example, a partially replaced building unit of PbI_xZ_{6-z} is found in $[PbI_2(4\text{-MPD})_2]_n$ (Fig. 47) [68], $[PbI_2(TMT)]_n$ [69], $[PbI_2(PYD)_2]_n$ [68], and $[PbI_2(2\text{-MPD})_2]_n$ [70]. An inorganic–organic hybrid layered structure is constructed with the help of the organic ligand, BIPY [71] (Fig. 48).

The length of the alkyl group can influence the dimension of the Pb/I anionic structure, for example, from a 2D layer (Fig. 49a) to a 1D chain (Fig. 49b). A simple structural relationship between $[PbI(S_2CNMe_2)]_n$ and $[PbI(S_2CNC_4H_8)]_n$ is illustrated in Fig. 49c; the stepped chain in $[PbI(S_2CNC_4H_8)]_n$ (Fig. 49c-(i)) forms a distorted hypothetical chain by displacement of some Pb-I bonds (Fig. 49c-(ii)), and the aggregation of such distorted chains gives the 2D layer in $[PbI(S_2CNMe_2)]_n$ [53].

Several aspects of the ligand, such as, coordination ability, flexibility, stereo effect, stacking of aromatic rings, and hydrogen bonding will also influence the M/I structure greatly. Therefore, these may provide some useful access to modification or to design a new iodometalate. Also, the organic ligand itself may be a source of desired properties. Explorations are worth trying.

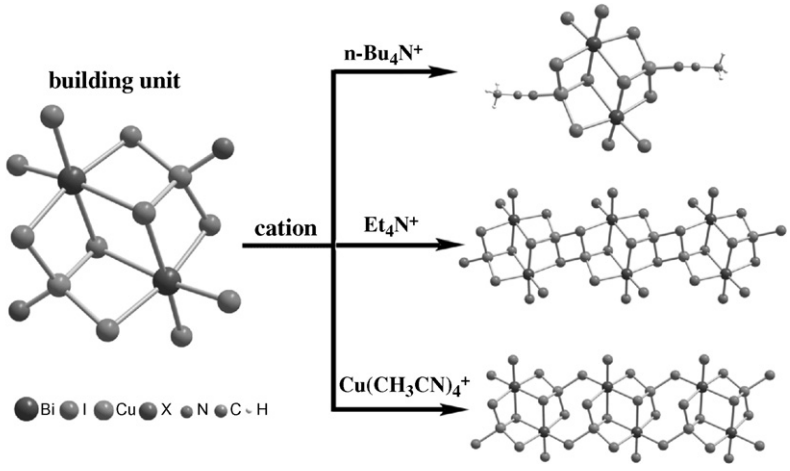

Fig. 46. Different anionic structures have been generated with the guidance with different cations from Ref. [67], with permission from the American Chemical Society.

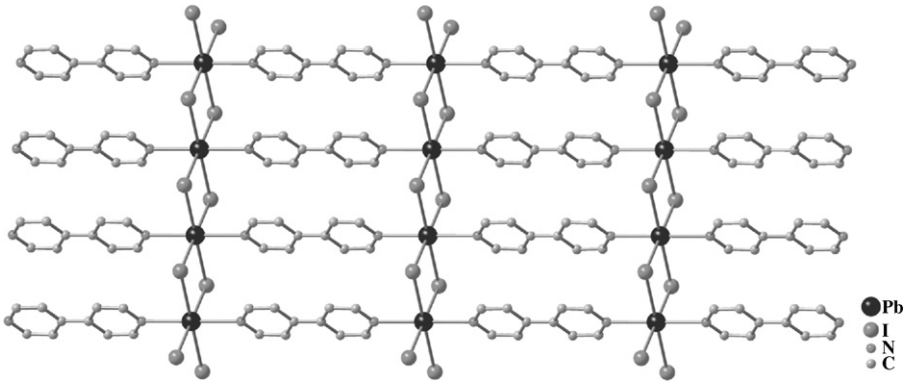

Fig. 48. Structure of layered $[PbI_2(4,4'\text{-BIPY})]_n$ [71].

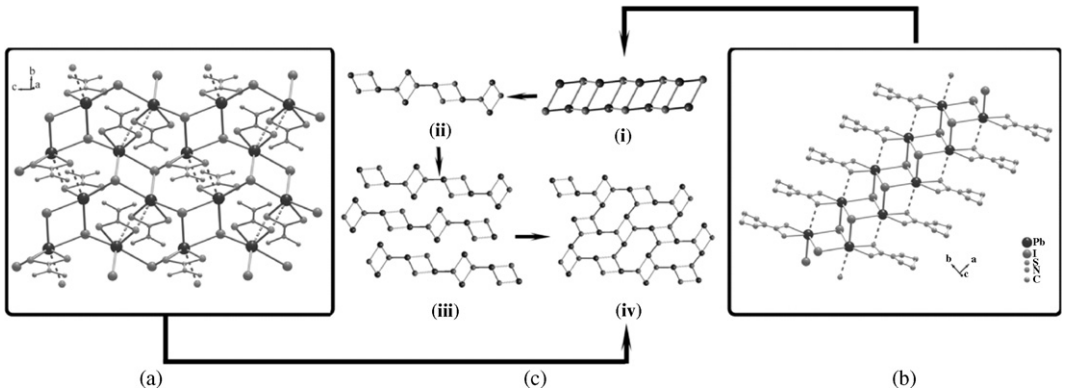

Fig. 49. The structure of (a) 2D layered structure in $[PbI(S_2CNMe_2)]_n$, (b) the 1D step chain structure in $[PbI(S_2CNC_4H_8)]_n$ and (c) structural relationship between step chain in (b) and layer in (a) [53].

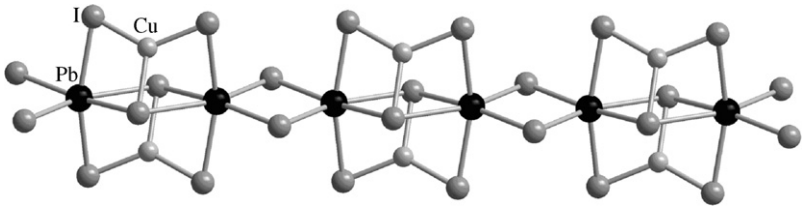

Fig. 50. Structure $[Bu_4N]_{4n}[PbCuI_4]_n$ [72].

4.3. Heterometal ion effect

4.3.1. Heterometal–iodine bonding effect

The cation effect has an indirect influence on the structure of the inorganic moiety, while the ligand effect can have either an indirect or direct influence. Another direct influence in this sense is the bonding interaction within the inorganic moiety. Several recent reports on the introduction of the d^{10} transition metal–iodine interactions into the Pb(Bi)/I systems have proven that TM–I bonding is an effective means to change the geometry and connection of the MI_6 octahedron and bring some new properties. Besides, the involvement of a second building unit, the TMI_4 tetrahedron, brings new possibilities for both connection and coordination sites for the ligands [66,67,72–74].

For example, the involvement of the trigonal coordinated Cu^+ ions leads to a significant distortion of the PbI_6 octahedron in $[Bu_4N]_n[PbCuI_4]_n$ (Fig. 50) [72]. Because of the large difference between the bond lengths of Cu–I and Pb–I, the Pb–I bonds are bent towards the Cu^+ ions by 19° from linear.

The Cu^+ ions introduced provide a coordination site for the ligand. Usually, Cu^+ tends to adopt a four-fold coordination polyhedron, therefore, when CH_3CN is present, the Cu^+ ion grabs CH_3CN to complete a tetrahedral coordination sphere as seen in compound $[PbI_4Cu_2(CH_3CN)_2]_n$ (Fig. 51) [75]. When a stronger ligand PPh_3 is presented, a very different structure, a bicubane-like cluster

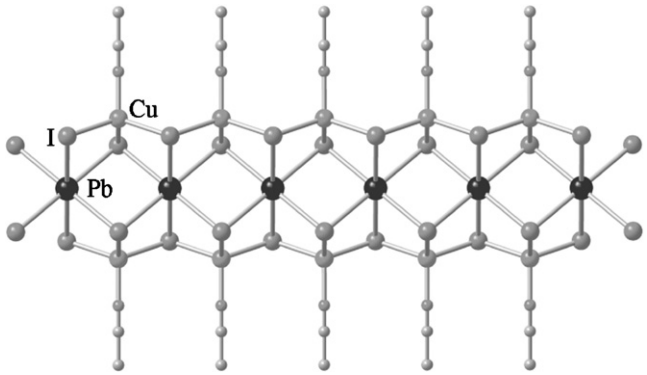

Fig. 51. Structure $[PbI_4Cu_2(CH_3CN)_2]_n$ [75].

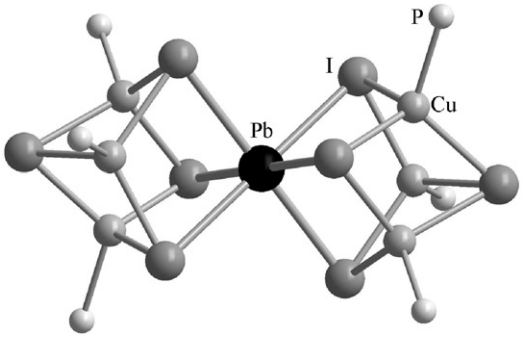

Fig. 52. Molecular structure of compound $PbCu_6I_8(PPh_3)_6$. For clarity, the PPh_3 molecules are omitted [72].

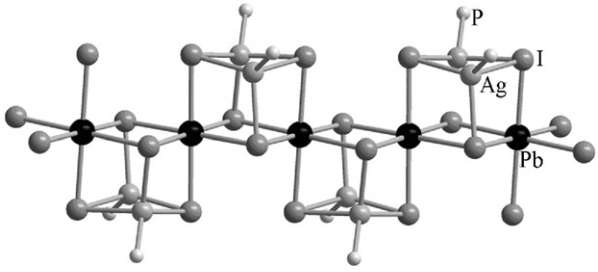

Fig. 53. Cubic chain $[PbAg_2(PPh_3)_2I_4]_n$ along *a* axis [72].

$[PbCu_6I_8(PPh_3)_6]$, is produced (Fig. 52) [72]. Again, the difference of radius between Pb^{2+} and Cu^+ ions leads to the distortion of the $PbCu_3I_4$ cubane. Interestingly, when a larger Ag^+ ion is utilized instead, the somewhat expected cubane-unit with less distortion occurs in $[PbAg_2(PPh_3)_2I_4]_n$ (Fig. 53) [72].

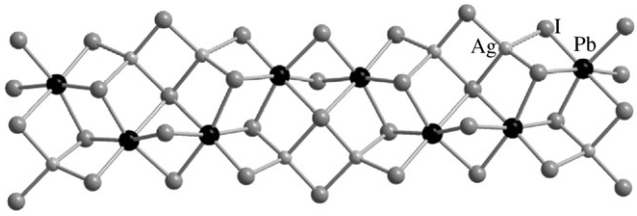

Fig. 54. Structure of 1D ribbon in $[Bu_4N]_n[PbAgI_4]_n$ along *b* axis [72].

As in $[Bu_4N]_n[PbAgI_4]_n$ (Fig. 54) [72], the PbI_6 octahedra are connected in a wavy chain motif accommodating the Ag_2I_6 dimer, which has not been found in any monometallic Pb/I polymers.

The different structural modifications generated by Ag^+ and Cu^+ ions are essentially related to the different sizes of Ag^+ and Cu^+, and the different bond energies of Ag–I and Cu–I bonds.

In addition, the charge of metal ion also brings about a structural change. For example, in $[(Bu_4N)_2Pb_6I_{18}Cu^{1+}{}_4Cu^{2+}(S_2CNMe_2)_2]_n$, (Fig. 55) Cu^{1+} has tetrahedral four-fold CuI_3S coordination environment with normal Cu–I bond of 2.61–2.70 Å, and a Cu–S bond of 2.34 Å, which serves as boundary atoms to stop the further extension of PbI_6 octahedra. Two such Cu^{1+}-confined ribbons are connected by planar four-fold coordinated Cu^{2+} cations to give a 2D layer [53].

The Bi/I system seems to be more flexible to accommodate either Cu^+ or Ag^+ ions. Compounds of $[Et_4N]_{2n}[Bi_2M_2I_{10}]_n$ M = Cu^+ or Ag^+ are isostructural, except that the BiI_6 octahedra are more distorted in the Ag-derivative (Fig. 56) [66,67].

The AgI_4 tetrahedron introduced can act as a structural linkage as in $[Et_4N]_{2n}[Bi_4Ag_2I_{16}]_n$ (Fig. 57) [66]. The common tetranuclear Bi_4I_{16} cluster is modified by four AgI_4 tetrahedra, which serve as linkages for the further extension into a 2D layer. Such a layer

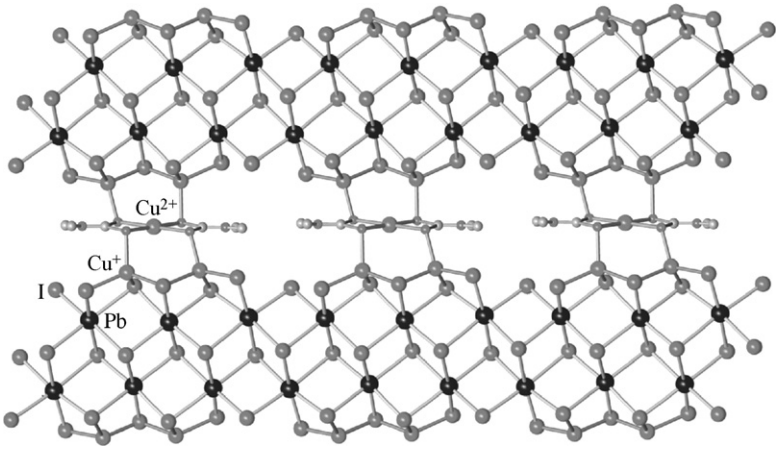

Fig. 55. Structure of anionic layer $[Bu_4N]_{2n}[Pb_6I_{18}Cu^{1+}{}_4Cu^{2+}(S_2CNMe_2)_2]_n$ [53].

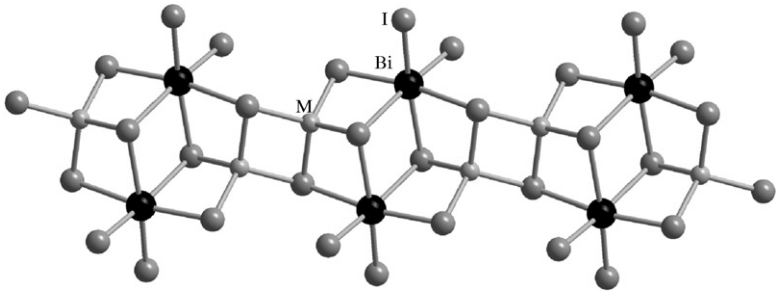

Fig. 56. Structure of $[Bi_2M_2I_{10}{}^{2-}]_n$ M = Cu or Ag [66,67].

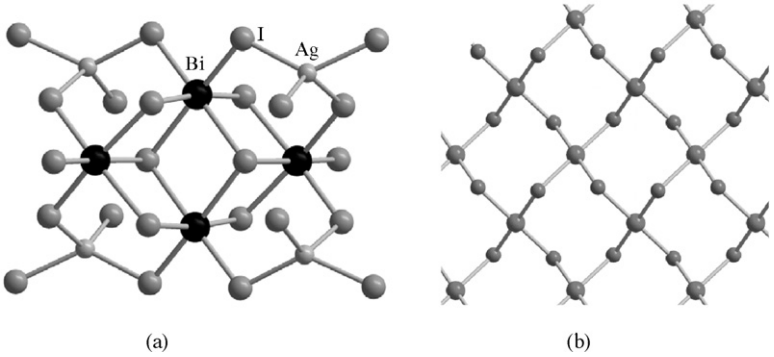

Fig. 57. (a) Structure of the anionic building unit $[Bi_4Ag_2I_{16}^{2-}]_n$ and (b) topological scheme of the layer in which the Bi_4I_{16} cluster is treated as a node, and the Ag atom as a linkage [66].

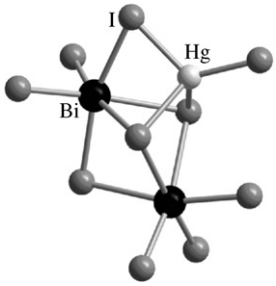

Fig. 58. Structure of trinuclear $[Bi_2HgI_{10}]^{2-}$ [76].

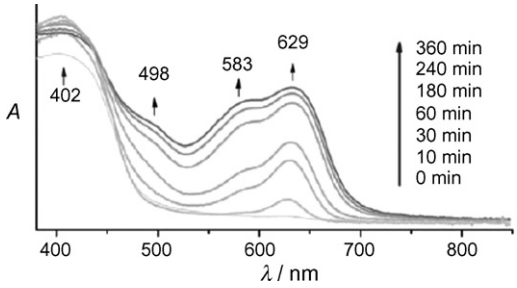

Fig. 60. Spectroscopic changes of $[EDAMP]_{2n}[Pb_7I_{18}]_n{\cdot}4nH_2O$ upon repeated irradiation at 300 nm at 25 °C. From Ref. [65], with permission from Wiley-VCH.

motif has not been observed in monometallic iodobismuthate or iodoplumbate, which suggests that the Ag–I bonding interactions are effective to create unprecedented structures.

4.3.2. Heterometal ion charge effect

A newly made trinuclear $[Bi_2HgI_{10}]^{2-}$ [76] anionic cluster (Fig. 58) structurally recalls a $[Pb_3I_{10}]^{4-}$ (Fig. 11) cluster in which the Pb-octahedra also share I–I–I face, but the 3rd Pb polyhedron (PbI_5 square pyramid) is replaced by a HgI_4 tetrahedron. Such a trinuclear $[Bi_2HgI_{10}]^{2-}$ cluster is isoelectronic with the tetranuclear building blocks in polymeric $[Bi_2Ag_2I_{10}^{2-}]_n$ [66], or $[Bi_2Cu_2I_{10}^{2-}]_n$ [67] (Fig. 56) but differs in that one divalent Hg^{2+} atom replaces the two Cu^+ (or Ag^+) atoms to regain the charge balance. An approximate dimerization of trinuclear $[Bi_2HgI_{10}]^{2-}$ generates a hexanuclear anionic $[Bi_4Hg_2I_{20}]^{4-}$cluster (Fig. 59) that is comparable to the known $[Bi_6I_{22}]^{4-}$ (Fig. 16) but differs in that this Bi/Hg cluster contains two I atoms less per formula. The reason is that two BiI_6 octahedra have been replaced by two HgI_4 tetrahedra. This dimerization is also different from that of $[Pb_7I_{22}]^{8-}$ (Fig. 19) in which the dimerization undergoes a different ($2[Pb_3I_{10}]^{4-} + [PbI_2]$) mode (Fig. 60).

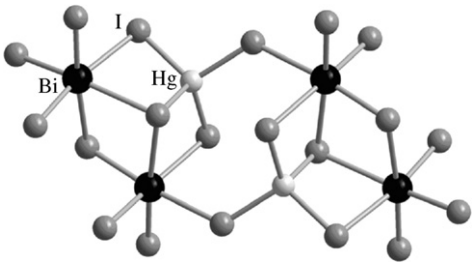

Fig. 59. Structure of hexanuclear $[Bi_4Hg_2I_{20}]^{4-}$ [76].

5. Various properties

The structural diversity of iodometalates is of great fundamental interest, while a search for interesting properties of the unprecedented compounds is another driving force for the research in this field.

5.1. Photochromism

An inorganic organic hybrid compound $[EDAMP]_{2n}[Pb_7I_{18}]_n{\cdot}4nH_2O$ (EDAMP = $Et_2NHC_6H_4CH_2C_6H_4NHEt_2$) (Fig. 44) [65], has shown interesting wavelength-dependent photochromism. Before and after visible irradiation ($\lambda = 550$ nm), the color of this compound changes from yellow to olive green. After further UV irradiation ($\lambda = 300$ nm), the color changes to dark green. The single crystal X-ray analyses reveal that there is no significant structural change in the inorganic moiety during the irradiation; only the organic species has subtle changes. The PbI_6 octahedron has built up a 3D inorganic open framework in which the sub building unit, an incomplete cubane chain, is thought to behave as an ordered and periodic quantum wire array that may contribute to the wavelength-dependent photochromic response.

5.2. The optical property related to the addition of M ion

The incorporation of Cu^+ ions with Pb coordination sphere leads to an unusual incomplete octahedron (with two vacant equatorial sites) in $PbI_4Cu_2(PPh_3)_4$ [73], Fig. 61a. The axial I–Pb–I angle is about 168°, around a 12° deviation from the ideal octahedral symmetry, and 14° larger than that in the monometallic cluster $[Bu_3N\text{-}(CH_2)_2\text{-}NBu_3][PbI_4]$, in which the axial I–Pb–I angle is 153.56°. DFT calculations have indicated that the increase of the electronegativity of iodine *via* the bonding interaction with copper ions causes such an axial angular difference.

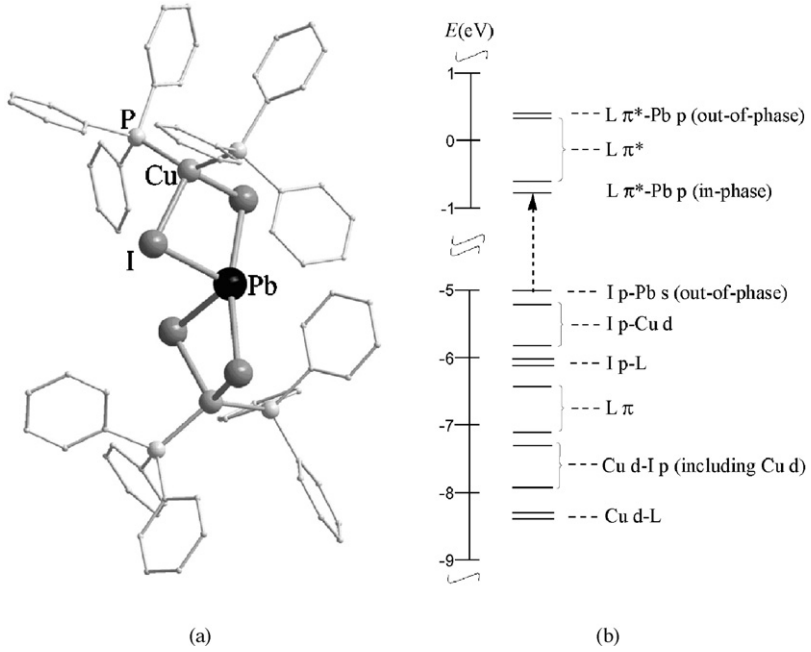

Fig. 61. (a) Structure of $PbCu_2I_4(PPh_3)_4$ [73] and (b) partial molecular orbital correlation diagram of $PbCu_2I_4(PPh_3)_4$. The arrow refers to the possible type of transition from the HOMO.

The optical band gap of $PbI_4Cu_2(PPh_3)_4$ is 2.69 eV, consistent with its yellow color. The solid-state emission spectrum of $PbI_4Cu_2(PPh_3)_4$ at 10 K is shown in Fig. 62. Excitation of the polycrystalline sample at $\lambda = 358$ nm produces an intense red-infrared emission with peak maximum at 732 nm ($\tau = 24$ μs). Based on the frontier molecular orbitals (MOs) calculation at the B3LYP level of DFT (Fig. 61b), the 732 nm emission band can be assigned as an iodine 5p-lead 6s to PPh_3-lead 6p charge transfer, i.e., halide and metal-to-ligand and metal charge transfer (XM-LM-CT).

The cluster $PbCu_6I_8(PPh_3)_6$ shown in Fig. 52 exhibits interesting optical properties. The photoluminescence peak at 690 nm with excitation wavelength (λ_{ex}) < 363 nm has a lifetime $\tau = 25$ μs. The luminescence peak at 542 nm with $\lambda_{ex} > 400$ nm has $\tau = 10$ μs (Fig. 63). The interesting near-infrared luminescence emission at 780 nm with $\lambda_{ex} > 400$ nm, has a lifetime $\tau = 17$ μs. The 780 nm emission has been assigned to be an I(5p)–Pb(6s) to PPh_3–Pb(6p) charge transition. The higher energy 690 nm emission originates from the cubane core. The hetero metal ions in such cubes and the relatively higher delocalized Pb–Cu and Cu–Cu interactions over the bicube cluster should have significant influence on such emissions. The 542 nm emission might be an exciton emission originating from the octahedral coordinated Pb^{2+} ion.

The cubic chain compound $[PbAg_2I_4(PPh_3)_2]_n$ shown in Fig. 53 has a yellow emission at 566 nm with $\tau = 12$ μs [72], which is around 3790 cm^{-1} red shifted compared with that of the isolated cubic cluster $Ag_4I_4(PPh_3)_4$ [77]. This emission might be assigned to a transition in the heterometallic cubane unit $[Ag_2Pb_2I_4^{2+}]$. The structure characteristics of these two compounds (1D cubic chain vs. discrete cubic cluster) suggest that the delocalization over the $Ag_2Pb_2I_4$ cube may be larger than that over the Ag_4I_4 cube, thus, the cube-related emission occurs at lower energy in the heterometallic Pb/Ag compound.

5.3. The band gap–dimension relationship

Recent study has shown a nice band gap–dimension of anionic moiety correlation. As shown in Fig. 64, the optical band

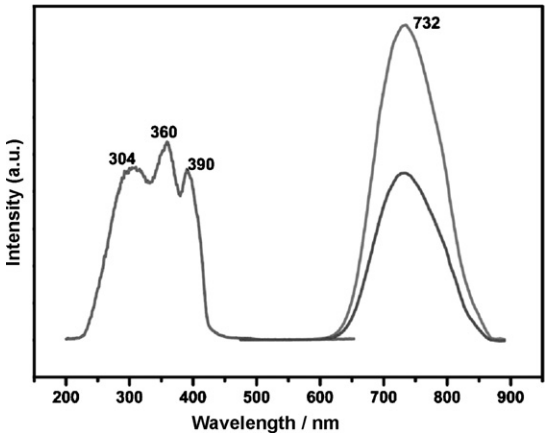

Fig. 62. The solid-state emission and excitation spectra of polycrystalline $PbI_4Cu_2(PPh_3)_4$ at 10 K (From Ref. [73], with permission from Elsevier.)

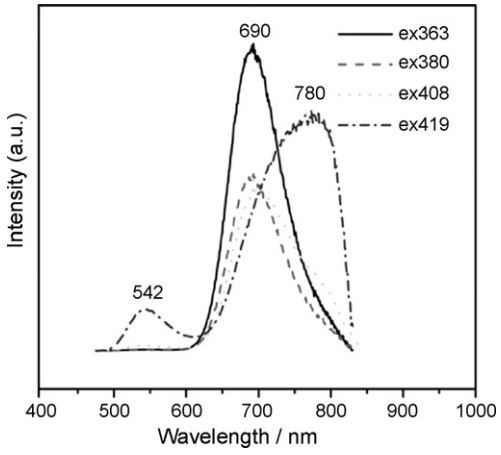

Fig. 63. Solid-state emission spectra of $PbCu_6I_8(PPh_3)_6$ at 10 K with representative peaks marked Adapted from Ref. [72], with permission from the American Chemical Society.

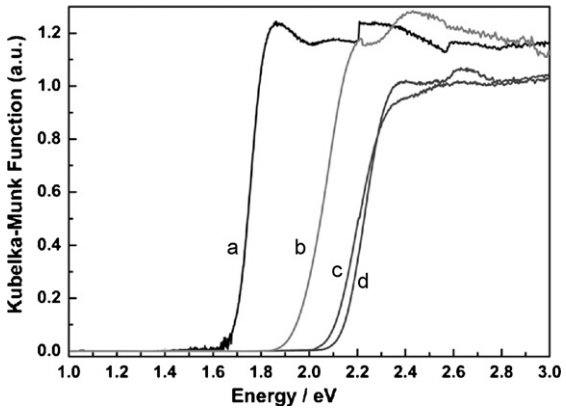

Fig. 64. Room-temperature optical absorption spectra for solid samples of (a) BiI_3, (b) $[Bu_4N]_{2n}[Bi_4I_{14}]_n$, (c) $[PhCH_2NEt_3]_4[Bi_4I_{16}]$, and (d) $[PhCH_2NEt_3]_3[Bi_2I_9]$. Adapted from Ref. [66].

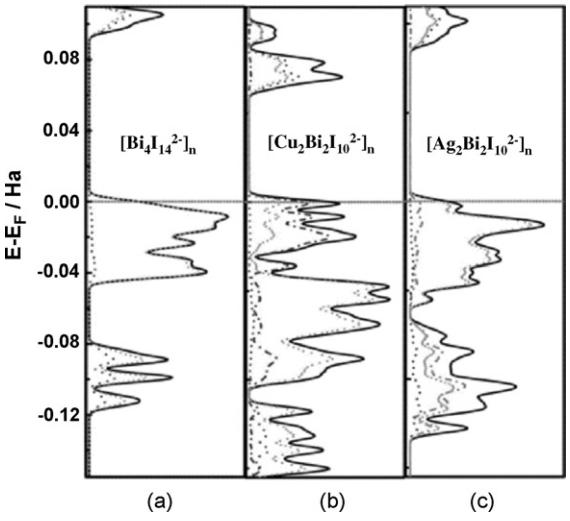

Fig. 65. Total and partial DOS plots of: (a) $[Bu_4N]_{2n}[Bi_4I_{14}]_n$, (b) $[Et_4N]_{2n}[Bi_2Cu_2I_{10}]_n$, and (c) $[Et_4N]_{2n}[Bi_2Ag_2I_{10}]_n$ with the Fermi levels set at zero. Solid lines represent total DOS and other lines represent the partial DOS, as follows: (dashed) Bi; (dot) I; (dash–dot) Cu [in (b)]; and (dash–dot) Ag [in (c)]. Adapted from Refs. [66,67].

gaps of dimeric $[PhCH_2NEt_3]_3[Bi_2I_9]$ (Fig. 6) [18], tetrameric $[PhCH_2NEt_3]_4[Bi_4I_{16}]$ (Fig. 12) [33], tetranuclear-unit 1D chain $(n\text{-}Bu_4N)_{2n}[Bi_4I_{14}]_n$ (Fig. 32) [41], and the binary iodides BiI_3, follow the trend of: dimeric $[Bi_2I_9]^{3-}$ (2.19 eV) > tetrameric $[Bi_4I_{16}]^{4-}$ (2.16 eV) > tetrameric unit-chain $[Bi_2Ag_2I_{10}{}^{2-}]_n$ (2.05 eV) > monometallic tetrameric unit-chain $[Bi_4I_{14}{}^{2-}]_n$ (2.02 eV). Such a gap reduction apparently follows an increase in the structural dimension of the anion. Furthermore, such an E_g reduction agrees with the increase of the corresponding M/r ratio from 0.27 for binuclear $[Bi_2I_{10}]^{4-}$ cluster to 0.67 for BiI_3 binary as listed in Table 1.

The E_g and M/r value correlation also holds for heterometallic compounds. For example, 1D $[Bi_2Ag_2I_{10}{}^{2-}]_n$ chain and 2D $[Bi_4Ag_2I_{16}{}^{2-}]_n$ layer, have $r = 4 + 2/2 + 4/3 = 6.33$, $M/r = 0.63$, and $r = 2 + 12/2 + 2/3 = 8.67$, $M/r = 0.69$, respectively. Their optical energy gaps are 2.05 and 1.93 eV [66], which decrease with increase in their M/r values.

Similar trends have also been found in Bi/I/Cu heterometallic compounds [67]. Red colored tetranuclear compound $[n\text{-}Bu_4N]_2[Bi_2Cu_2(CH_3CN)_2I_{10}]$ has $E_{g(obs)} = 2.06$ eV, $E_{g(cal)} = 2.02$ eV, $r = 4 + 4/2 + 2/3 = 6.67$, and $M/r = 0.60$. The dark red colored linear chain $[Et_4N]_{2n}[Bi_2Cu_2I_{10}]_n$ has $E_{g(obs)} = 1.89$ eV, $E_{g(cal)} = 1.86$ eV, $r = 4 + 4/2 + 2/3 = 6.67$, and $M/r = 0.63$. The black colored thicker linear chain $[Cu(CH_3CN)_4]_{2n}[Bi_2Cu_2I_{10}]_n$ has $E_{g(obs)} = 1.80$ eV, $E_{g(cal)} = 1.90$ eV, $r = 4 + 4/2 + 2/3 = 6.67$, and $M/r = 0.71$. The clear decrease of E_g in these compounds is consistent with the color darkening from red to black, and such a trend fits nicely to the increase in M/r values. Note that the calculated E_g values of the two linear compounds deviate noticeably from the observed values because of the inaccuracy of the DFT calculation method on the estimation of E_g. In these cases M/r values seem to fit experiments better. Therefore the M/r value would be a simple structural indicator as a very useful complementary parameter to evaluate the property.

5.4. Contribution of Cu^+ or Ag^+ to the band structure

Isostructural compounds $[Et_4N]_{2n}][Bi_2Ag_2I_{10}]_n$ and $[Et_4N]_{2n}[Bi_2Cu_2I_{10}]_n$ (Fig. 56) have the same M/r value (0.63). However, their band gaps are different (2.05 and 1.89 eV) [66,67]. The DFT calculations revealed that such a band gap difference originates from the different contributions of Cu^+ and Ag^+ ions to the electronic structure. As a comparison, the band structure of the monometallic isostructural $[n\text{-}Bu_4N]_{2n}[Bi_4I_{14}]_n$ is shown in Fig. 65a. The highest occupied crystal orbital (HOCO) is made from Bi–I bonding states, I nonbonding states; and the lowest unoccupied crystal orbital (LUCO) is constituted with Bi–I antibonding states. In the $[Bi_2Cu_2I_{10}{}^{2-}]_n$ anion, Fig. 65b, the I nonbonding and Bi–I antibonding states in HOCO show no significant energetic changes, but the Cu–I antibonding states have now been inserted between HOCO and LUCO. Accordingly, the tops of the valence bands of the Cu analogs now derive nearly entirely from I and Cu orbitals, and consequently, the energy gaps have decreased (1.89 eV for Cu analog vs. 2.02 eV for monometallic $[Bi_4I_{14}{}^{2-}]_n$). Dissimilarly, the lower energy lying Ag^+ in Ag analog (Fig. 65c) does not influence the components of the HOCO. Thus the energy gap is 2.05 eV, only 0.03 eV larger than that for $[n\text{-}Bu_4N]_{2n}[Bi_4I_{14}]_n$, an increase that might derive from the overall distortion of Bi–I skeleton by the involvement of Ag^+ ions.

5.5. Distinct thermal stabilities

Studies have shown that the thermal stabilities of Bi/Cu heterometallic iodobismuthates are determined by the Bi: I: Cu ratio and the involvement of solvent molecule [67]. Three similar compounds shown in Fig. 46 have distinct thermal stabilities. The isolated cluster $[Bu_4N]_2[Bi_2Cu_2(CH_3CN)_2I_{10}]$ loses CH_3CN ligands around 85 °C, and ends up with a "$(Bu_4N)_2(Cu_2Bi_2I_{10})$" composition, which is still a thermally stable phase. Such "$(Bu_4N)_2(Cu_2Bi_2I_{10})$" has changed to an unknown phase which melts congruently at 145 °C, and decomposes above 230 °C (Fig. 66). Contrarily, the linear and solvent free $[Et_4N]_{2n}[Bi_2Cu_2I_{10}]_n$ is stable up to 230 °C, and no phase transition or decomposition is found. Linear compound $[Cu(CH_3CN)_4]_{2n}[Bi_2Cu_2I_{10}]_n$ loses coordinated CH_3CN molecules about 80 °C and decomposes to trigonal BiI_3 plus cubic CuI. Such a low decomposition temperature is caused by the resultant CH_3CN-free composition of "$Bi_2Cu_4I_{10''}$ is unstable with respect to the simple binary iodides [67].

5.6. Interesting ferroelectric property

Ferroelectric materials possess a permanent dipole moment, which is reversible in the presence of an applied voltage. This kind of material is required to adopt a space group belonging to one of the ten polar point groups (C_1, C_s, C_2, C_{2v}, C_3, C_{3v}, C_4, C_{4v}, C_6, C_{6v}). Usually, the ferroelectric materials are assorted as oxides, non-oxide inorganic crystals, organic crystals, liquid crystals, and polymers [78].

Recent studies have found that the iodobismuthate has a relatively greater chance to find a polar structure and therefore would

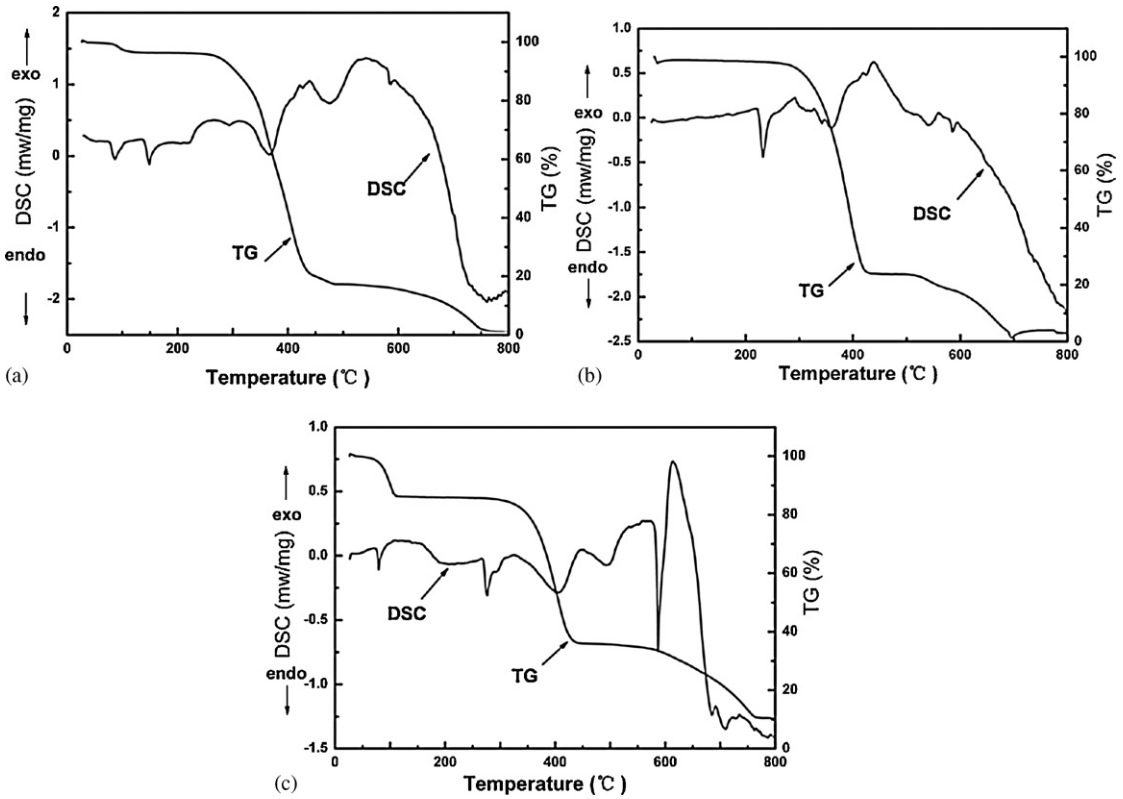

Fig. 66. TG/DSC curves of compounds (a) $[Bu_4N]_2[Bi_2Cu_2(CH_3CN)_2I_{10}]$, (b) $[Et_4N]_{2n}[Bi_2Cu_2I_{10}]_n$, and (c) $[Cu(CH_3CN)_4]_{2n}[Bi_2Cu_2I_{10}]_n$. From Ref. [67], with permission from the American Chemical Society.

be a novel system for the exploration of the possible ferroelectric materials. For example, $BiI_6Cu_3(PPh_3)_6$ [79] has a Bi atom with an extremely distorted octahedral geometry with a maximum axial-to-equatorial angular deviation of 29° to ideal 90°. Such distortion may be related to the capping of CuI_2P_2 tetrahedron. Isostructural $BiI_6Ag_3(PPh_3)_6{\cdot}3H_2O$ [79] has less distortion around Bi center, i.e. 17° deviation of axial-to-axial angle to ideal 180°. Such distortion is driven by the unmatched bond length of Ag/Cu–I to Bi–I.

These two compounds crystallize in orthorhombic ($Pna2_1$) and trigonal ($R3c$) systems, respectively, which belong to the polar point groups (C_{2v} and C_{3v}) required for the ferroelectric materials. Their ferroelectric hysteresis loops measured on pellets of the crystalline sample at room temperature, indicate the remanent polarization (Pr, μC/cm^2) and coercive field (Ec, kV/cm) of ca.0.008, 0.017; and 5, 8 respectively.

Other polarized iodobismuthates have been found recently, such as $[Cu_3(p\text{-}bix)_3]_n[Bi_2I_9]_n$ $P1$ space group [79], and the polycrystalline sample shows Pr = 0.0085 μC/cm^2, Ps = 0.017 μC/cm^{2}and Ec = ~6.6 kV/cm. The permanent polarization of Bi/M/I system may originate with the flexibility of the large and soft central Bi atoms and the high degree of the distortion tolerance of the BiI_6 octahedron. More work is worthwhile.

6. Summary

The structural types of iodoplumbates and iodobismuthates have been summarized according to their dimensionality. For 0D discrete monometallic clusters, the nuclearity can be 1–8, 10 and 18. The different connections of the MI_6 (M = Pb, Bi) octahedron generate 1D polymers with different configurations *via* sharing faces, edges, or apexes. The extension of the building unit in more directions generates 3D open framework or 2D polymers or hybrid 2D layers with the aids of organic linkages. To some degree, the structures of iodometalates are controllable by the cation effect, ligand effect and heterometallic-iodine bonding effect.

An empirical M/r value has been proposed for the first time. Such an M/r value is useful to evaluate ADIM and the properties of iodometalates. In addition, the M/r values of different examples invariably increase with a decrease of the energy gaps, which is in good agreement with their apparent color changes, and the electronic structure analyses. The M/r values may be a key to access the design and rational syntheses of novel iodometalates, and such empirical rules are expected to be suitable in other systems, such as Sn/I, M/X (X = F, Cl, Br) or TM/Ch (TM = transition metal, Ch = chalcogen).

Several property–structure relationships, such as luminescence related to the structural configuration, distortion and heterometallic bonding interactions; thermal stability variations with the dimensionality and composition; energy gap-to-ADIM correlation; and ferroelectricity arising from the flexibility and distortion are discussed. The different contributions of heterometallic cations to the band structures are also presented.

One of the charms of chemistry is the ability for rational synthesis to access the target compound with a desired property, which is based on a thorough understanding of the structure and property–structure relationship. Iodometalate is such a system deserving of continuous exploration.

Acknowledgements

We thank J.-P. Li, and M.-W. Yuan for their help in drawing some pictures. This research was supported by the National Natural Science Foundation of China under Projects (20773130, 20733003, 20821061), the "Key Project from CAS" (KJCX2-YW-H01), 973 Program (2009CB939801) and the "Key Project from FJIRSM" (SZD08002).

References

[1] X.H. Zhu, Z.R. Wei, Y.R. Jin, A.P. Xiang, Cryst. Res. Technol. 42 (2007) 456.
[2] A.M. Goforth, J.R. Gardinier, M.D. Smith, L. Peterson, H.C.Z. Loye, Inorg. Chem. Commun. 8 (2005) 684.
[3] M.V. Artemyev, Y.P. Rakovich, G.P. Yablonski, J. Cryst. Growth 171 (1997) 447.
[4] K. Tanaka, T. Hosoya, R. Fukaya, J. Takeda, J. Lumin. (2007), 122–123, 421.
[5] M. Baibarac, N. Preda, L. Mihut, I. Baltog, S. Lefrant, J.Y. Mevellec, J. Phys.: Condens. Mater. 16 (2004) 2345.
[6] E. Lifshitz, M. Yassen, L. Bykov, I. Dag, J. Phys. Chem. 98 (1994) 1459.
[7] D. Sarid, B.R. Phee, B.P. McGinnis, Appl. Phys. Lett. 49 (1986) 1196.
[8] V. Deich, M. Roth, Nucl. Instrum. Methods Phys. Res. A 380 (1996) 169.
[9] A. Cuna, A. Noguera, E. Saucedo, L. Fornaro, Cryst. Res. Technol. 39 (2004) 912.
[10] G.E. Jellison, J.O. Ramey, A.A. Boatner, Phys. Rev. B: Condens. Matter 59 (1999) 9718.
[11] A. Cuna, I. Aguiar, A. Gancharov, M. Perez, L. Fornaro, Cryst. Res. Technol. 39 (2004) 899.
[12] H. Krautscheid, F. Vielsack, Angew. Chem. Int. Ed. Engl. 34 (1995) 2035.
[13] H. Krautscheid, F. Vielsack, J. Chem. Soc., Dalton Trans. (1999) 2731.
[14] H. Krautscheid, C. Lode, F. Vielsack, H. Vollmer, J. Chem. Soc., Dalton Trans. (2001) 1099.
[15] G.A. Fisher, N.C. Norman, Adv. Inorg. Chem. 41 (1994) 233.
[16] T. Hattori, T. Taira, M. Era, T. Tsutsui, S. Saito, Chem. Phys. Lett. 254 (1996) 103.
[17] M. Era, S. Morimoto, T. Tsutsui, S. Saito, Appl. Phys. Lett. 65 (1994) 676.
[18] A.M. Guloy, Z.J. Tang, P.B. Miranda, V.I. Srdanov, Adv. Mater. 13 (2001) 833.
[19] H. Eickmeier, B. Jaschinski, A. Hepp, J. Nuss, H. Reuter, R. Blachnik, Z. Naturforsch. B: J. Chem. Sci. 54 (1999) 305.
[20] T. Devic, M. Evain, Y. Moëlo, E. Canadell, P.A. Senzier, M. Fourmigué, P. Batail, J. Am. Chem. Soc. 125 (2003) 3295.
[21] T. Devic, E. Canadell, P. Auban-senzier, P. Batail, J. Mater. Chem. 14 (2004) 135.
[22] W. Medycki, R. Jakubas, N. Pislewski, J. Lefebvre, Z. Naturforsch. A: Phys. Sci. 48 (1993) 748.
[23] G.C. Papavassiliou, I.B. Koutselas, A. Terzis, C.P. Raptopoulou, Z. Naturforsch. B: Chem. Sci. 50 (1995) 1566.
[24] B.R. Vincent, K.N. Robertson, T.S. Cameron, O. Knop, Can. J. Chem. 65 (1987) 1042.
[25] H. Krautscheid, F. Vielsack, Z. Anorg. Allg. Chem. 625 (1999) 562.
[26] H. Krautscheid, Z. Anorg. Allg. Chem. 625 (1999) 192.
[27] O. Lindqvist, Acta Chem. Scand. 22 (1968) 2943.
[28] B. Chabot, E. Parthe, Acta Crystallogr. B: Struct. Sci. 34 (1978) 645.
[29] C. Feldmann, Z. Kristallogr.: N. Cryst. Struct. 216 (2001) 465.
[30] G.A. Bowmaker, P.C. Junk, A.M. Lee, B.W. Skelton, A.H. White, Austr. J. Chem. 51 (1998) 293.
[31] U. Geiser, E. Wade, H.H. Wang, J.M. Williams, Acta Crystallogr. C: Cryst. Struct. Commun. 46 (1990) 1547.
[32] A. Okrut, C.Z. Feldmann, Anorg. Allg. Chem. 632 (2006) 409.
[33] R. Kubiak, K. Ejsmont, J. Mol. Struct. 474 (1999) 275.
[34] C.J. Carmalt, L.J. Farrugia, N.C. Norman, Z. Naturforsch. B: Chem. Sci. 50 (1995) 1591.
[35] S. Pohl, M. Peters, D. Haase, W. Saak, Z. Naturforsch. B: Chem. Sci. 49 (1994) 741.
[36] V.V. Sharutin, I.V. Egorova, O.K. Sharutina, O.A. Dorofeeva, T.K. Ivanenko, A.V. Gerasimenko, M.A. Pushilin, Russ. J. Coord. Chem. 30 (2004) 874.
[37] H. Krautscheid, Z. Anorg. Allg. Chem. 620 (1994) 1559.
[38] W. Clegg, R.J. Errington, G.A. Fisher, M.E. Green, D.C.R. Hockless, N.C. Norman, Chem. Ber. 124 (1991) 2457.
[39] H. Eickmeier, B. Jaschinski, A. Hepp, J. Nuss, H. Reuter, R. Blachnik, Z. Naturforsch. B: Chem. Sci. 54 (1999) 305.
[40] A.M. Goforth, M.A. Tershansy, M.D. Smith, L. Peterson, H.C.Z. Loye, Acta Crystallogr. C: Cryst. Struct. Commun. 62 (2006) M381.
[41] H. Krautscheid, Z. Anorg. Allg. Chem. 621 (1995) 2049.
[42] C. Feldmann, J. Solid State Chem. 172 (2003) 53.
[43] Z.J. Tang, A.M. Guloy, J. Am. Chem. Soc. 121 (1999) 452.
[44] S.S. Nagapetyan, A.R. Arakelova, E.A. Ziger, V.M. Koshkin, Y.T. Struchkov, V.E. Shklover, Russ. J. Inorg. Chem. (Transl. Zh. Neorg. Khim.) 34 (1989) 2244.
[45] A. Cornia, A.C. Fabretti, R. Grandi, W. Malavasi, J. Chem. Crystallogr. 24 (1994) 277.
[46] S. Chaabouni, S. Kamoun, J. Jaud, J. Chem. Crystallogr. 27 (1997) 527.
[47] S.M. Wang, D.B. Mitzi, C.A. Feild, A.M. Guloy, J. Am. Chem. Soc. 117 (1995) 5297.
[48] G.C. Papavassiliou, G.A. Mousdis, C.P. Raptopoulou, A. Terzis, Z. Naturforsch. 54b (1999) 1405.
[49] G.A. Mousdis, G.C. Papavassiliou, A. Terzis, C.P. Raptopoulou, Z. Naturforsch. B: Chem. Sci. 53 (1998) 927.
[50] Z.J. Zhang, G.C. Guo, G. Xu, M.L. Fu, J.P. Zou, J.S. Huang, Inorg. Chem. 45 (2006) 1972.
[51] H. Krautscheid, F. Vielsack, Z. Anorg. Allg. Chem. 623 (1997) 259.
[52] H. Krautscheid, J.F. Lekieffre, J. Besinger, Z. Anorg. Allg. Chem. 622 (1996) 1781.
[53] L.Q. Fan, L.M. Wu, L. Chen, unpublished work.
[54] J. Calabrese, N.L. Jones, R.L. Harlow, N. Herron, D.L. Thorn, Y. Wang, J. Am. Chem. Soc. 113 (1991) 2328.
[55] D.B. Mitzi, Chem. Mater. 8 (1996) 791.
[56] N. Mercier, Cryst. Eng. Commun. 7 (2005) 429.
[57] X.H. Zhu, N. Mercier, A. Riou, P. Blanchard, P. Frère, Chem. Commun. (2002) 2160.
[58] D.B. Mitzi, J. Chem. Soc., Dalton Trans. (2001) 1.
[59] D.B. Mitzi, C.A. Feild, W.T.A. Harrison, A.M. Guloy, Nature 369 (1994) 467.
[60] T. Ishihara, J. Lumin. 60–61 (1994) 269.
[61] J.M. Harrowfield, H. Miyamae, B.W. Skelton, A.A. Soudi, A.H. White, Aust. J. Chem. 49 (1996) 1157.
[62] Z.J. Zhang, G.C. Guo, G. Xu, M.L. Fu, J.P. Zou, J.S. Huang, Inorg. Chem. 45 (2006) 10028.
[63] J.P. Li, L.H. Li, L.M. Wu, L. Chen, Inorg. Chem. 48 (2009) 1260.
[64] H. Krautscheid, F. Vielsack, N. Klaassen, Z. Anorg. Allg. Chem. 624 (1998) 807.
[65] Z.J. Zhang, S.C. Xiang, G.C. Guo, G. Xu, M.S. Wang, J.P. Zou, S.P. Guo, J.S. Huang, Angew. Chem. Int. Ed. 47 (2008) 4149.
[66] W.X. Chai, L.M. Wu, J.Q. Li, L. Chen, Inorg. Chem. 46 (2007) 1042.
[67] W.X. Chai, L.M. Wu, J.Q. Li, L. Chen, Inorg. Chem. 46 (2007) 8698.
[68] H. Miyamae, H. Toriyama, T. Abe, G. Hihara, M. Nagata, Acta Crystallogr. C: Cryst. Struct. Commun. 40 (1984) 1559.
[69] H. Miyamae, G. Hihara, K. Hayashi, M. Nagata, J. Chem. Soc. Jpn. (1986) 1501.
[70] L.M. Engelhardt, J.M. Patrick, C.R. Whitaker, A.H. White, Aust. J. Chem. 40 (1987) 2107.
[71] Y.J. Shi, Y. Xu, Y. Zhang, B. Huang, D.R. Zhu, C.M. Jin, H.G. Zhu, Z. Yu, X.T. Chen, X.Z. You, Chem. Lett. (2001) 678.
[72] L.Q. Fan, L.M. Wu, L. Chen, Inorg. Chem. 45 (2006) 3149.
[73] L.Q. Fan, Y.Z. Huang, L.M. Wu, L. Chen, J.Q. Li, E. Ma, J. Solid State Chem. 179 (2006) 2361.
[74] M.C. Burns, M.A. Tershansy, J.M. Ellsworth, Z. Khaliq, L. Peterson, M.D. Smith, H.C.Z. Loye, Inorg. Chem. 45 (2006) 10437.
[75] H. Hartl, M. Hoyer, Z. Naturforsch. B: Chem. Sci. 52 (1997) 766.
[76] M.W. Yuan, L.H. Li, L. Chen, Z. Anorg. Allg. Chem. (2009) 635, in press.
[77] M. Henary, J.I. Zink, Inorg. Chem. 30 (1991) 3111.
[78] W. Zhang, H.Y. Ye, R.G. Xiong, Metal-organic coordination compounds for potential ferroelectrics, Coord. Chem. Rev. 253 (2009) 2980.
[79] W.X. Chai, L.M. Wu, J.Q. Li, L. Chen, unpublished work.